American Journal of Science

GEOMORPHIC EXPRESSION OF ACTIVE TECTONICS IN A RAPIDLY-DEFORMING FOREARC, SILA MASSIF, CALABRIA, SOUTHERN ITALY

PAOLA MOLIN*, FRANK J. PAZZAGLIA** and FRANCESCO DRAMIS*

ABSTRACT.   We examine the tectonic geomorphology of La Sila, Calabria, southern Italy, a high-standing (1500 m) plateau surrounded by crustal extension, with map, DEM, and field data. These data are used to constrain a simple geodynamic model that describes short-wavelength deformation of the plateau rim. Topographic metrics including drainage patterns, river longitudinal profiles, and swath profiles are consistent with field stratigraphic relationships collectively suggesting that local tectonic deformation is embedded within a broader, regional uplift that has increased the mean elevation of the Sila Plateau during the Quaternary. The concavity, steepness, and length-gradient index of modeled river longitudinal profiles proved to be the most useful metrics for recording the effects of locally active faults. A previously unrecognized horst on the northeastern portion of the plateau was identified with these data. Nevertheless, the core of the Sila Plateau remains relatively undeformed with respect to its flanks which are characterized by steep, fault-bounded escarpments. Active extension has dropped base level for and unloaded the plateau rim, causing deep fluvial incision and associated flexural uplift of the footwall. This footwall uplift helps maintain a separate external, and nearly radial drainage away from the plateau along its flanks, and a nearly closed drainage for the plateau interior. A drainage divide roughly correlates with the plateau rim, inhibiting the process of drainage integration through the Sila interior and subsequent landscape dissection. As a result, geomorphic processes driving erosion of the Sila upland are lagging behind the tectonic processes that have driven rock uplift leading to an overall increase in mean surface elevation. These results underscore the importance of the lag times a landscape may endure in transforming from one tectonic and base level condition to another. We conclude that the Calabrian forearc has a similar geomorphic evolution as the more northern Apennines consistent with the emerging view that growth of Apennine topography has been recent (Quaternary), rapid, and possibly decoupled from rock deformation in the orogenic wedge.

INTRODUCTION

The relationship between plate convergence, crustal shortening, and emergence of topography in active orogens continues to be a topic of lively debate (Hovius, 2000; Willett and others, 2001). In the Italian Apennines, geologic and geomorphic data suggest that topographic emergence proceeded slowly during the major phase of crustal shortening throughout the Miocene and Pliocene, but accelerated significantly in the Quaternary as the rate of shortening has slowed (Ciaranfi and others, 1983; Castellarin and others, 1985; Colella and others, 1987; Dramis, 1992; Moretti, 1993; Thomson, 1994; Tortorici and others, 1995; Argnani and others, 1997; Bertotti and others, 1997; Moretti and Guerra, 1997; Carminati and others, 1999; Calamita and

*Dipartimento di Scienze Geologiche, Università degli Studi "Roma Tre," Largo S. Leonardo Murialdo, 1,00146 Roma, Italia; p.molin@geo.uniroma3.it
**Department of Earth and Environmental Science, Lehigh University, 31 Williams Dr., Bethlehem, Pennsylvania 18015; fjp3@Lehigh.edu

others, 1999; Coltorti and Pieruccini, 2000). Disparate rates of topographic growth (rock uplift above sea level) in an emergent forearc ideally would impart a unique fingerprint in the resulting landforms where they can be interpreted in terms of active tectonic processes (for example Wells and others, 1988). A good place within the Apennines to investigate the geomorphic expression of active tectonics is northern Calabria (fig. 1), the "toe of the boot" in southern Italy and the southernmost segment of the chain (fig. 1). Here, the emergent part of the range is narrow, rugged, underlain by a relatively uniform rock type, and is strongly arcuate, bending from a northwest-southeast to a northeast-southwest orientation (fig. 1A). Previous and ongoing studies provide some background for reconstructing the general tectonic and erosional unroofing setting (Thomson, 1994; Rossetti and others, 2001) and absolute uplift of rocks with respect to sea level (Gliozzi, ms, 1988; Palmentola and others, 1990; Carobene and Dai Prà, 1990; Cucci and Cinti, 1998; Molin and others, 2002).

This paper examines the tectonic geomorphology of the northern portion of the Sila Plateau in Calabria (fig. 2), focusing on the landscape morphometry, drainage patterns, and river longitudinal profiles in the context of an actively deforming forearc. We couple map- and DEM-based topographic analyses with field observations to help constrain a simple geodynamic model that characterizes the tectonic influence on the geomorphology and landscape evolution. Our goal is to discern between the regional tectonic processes at a convergent margin that drive regional rock uplift and subsidence, and to investigate the local adjustments of streams and drainage patterns to local deformational processes. The results are consistent with a landscape dominated by crustal extension including block tilting and flexure of footwall uplifts, coincident with regional relative base level fall (rock and surface uplift). Using these results we develop a conceptual model for the long-term landscape evolution of the Apennine arc through Calabria that places some limits on geodynamic considerations of how and when the forearc emerges in this setting.

GEOLOGIC AND PHYSIOGRAPHIC SETTING

The Apennines are a local expression of the convergence between the African and European plates in the Mediterranean region. In the late Oligocene, Hercynian crystalline rocks currently located in diverse localities throughout the western Mediterranean region (Corsica, Sardinia, Calabria, Sicily, northern Africa, southern Spain) were part of an orogenic wedge within a north-dipping subduction zone along the southern European margin (Lonergan and White, 1997). Between 35 and 30 Ma, an acceleration in the rollback of the subducting slab commenced as the absolute northward motion of the African plate decreased with the closing of the western Mediterranean basin (Jolivet and Faccenna, 2000). The result was the opening of a backarc basin (the Ligurian-Provençal basin) and the eastward rotation of a large piece of Hercynian crust to become the Sardinia-Corsica block. This block stranded on the southeastern margin of the backarc between 30 and 16 Ma (Ogniben, 1973; Malinverno and Ryan, 1986; Knott, 1987; Royden and others, 1987; Patacca and others, 1990; Lonergan and White, 1997; Jolivet and Faccenna, 2000; Faccenna and others, 2001) (fig. 1A). An accretionary prism formed in front of (to the east and south) and beneath the Sardinia-Corsica block, now part of a new forearc high, as extension dominated in the backarc (Malinverno and Ryan, 1986; Patacca and Scandone, 1989; Patacca and others, 1990). At around 10 Ma, the opening of the Tyrrhenian basin in the backarc further dissected the Sardinia-Corsica block forming a separate Calabria block and initiated the modern eastward migration of the Apennine forearc basins (Malinverno and Ryan, 1986; Patacca and Scandone, 1989; Patacca and others, 1990; Mantovani and others, 1996; Faccenna and others, 2001). This extension event is well constrained by coeval Tortonian syn-rift sedimentary rocks preserved at the margins of both Sardinia and Calabria blocks, and by the formation of oceanic crust in the Tyrrhenian basin
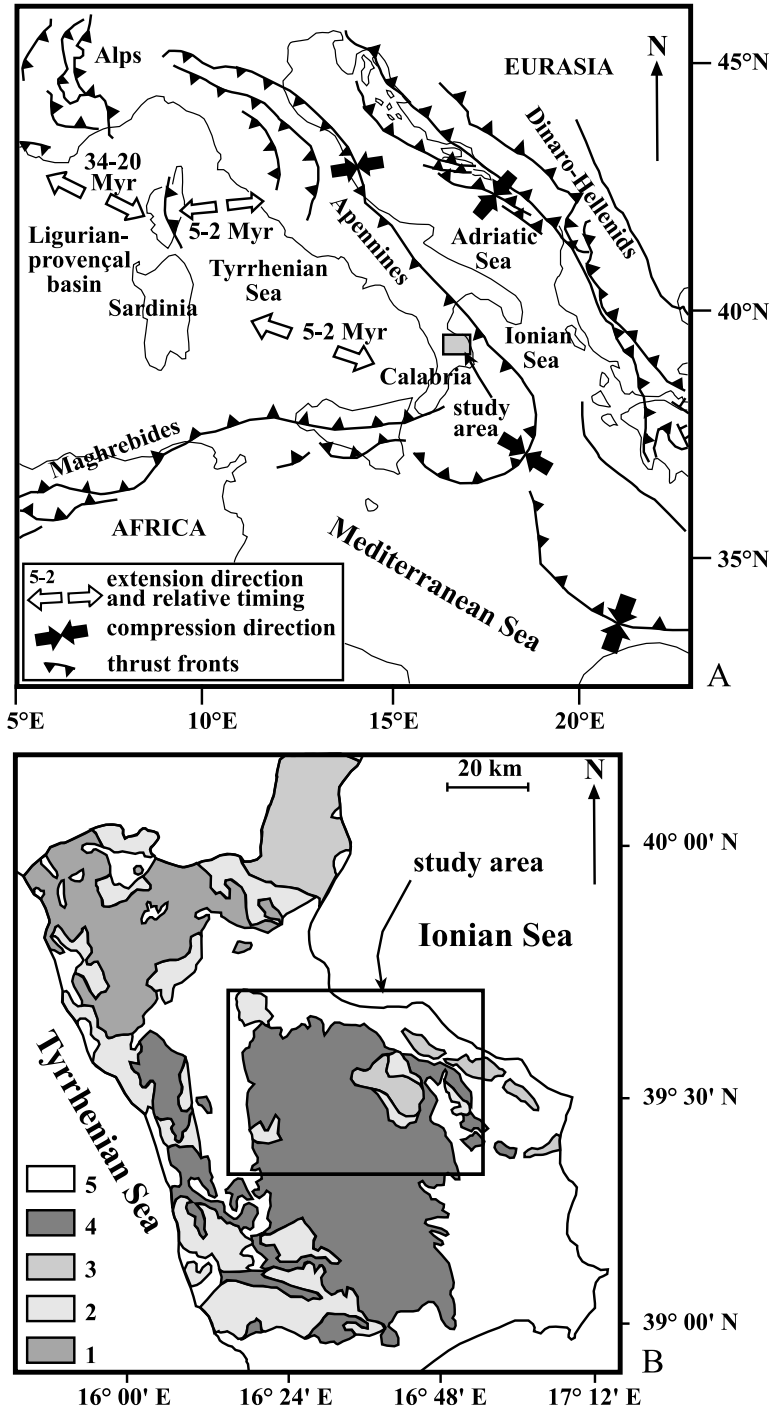
Fig. 1. (A) Simplified tectonic map of central Mediterranean (modified from Lonergan and White (1997); Rossetti and others, (2001)) and location of study area. (B) Simplified geologic map of Northern Calabria and location of the study area: (1) Apenninic carbonate units; (2) low-grade metamorphic units and ophiolites; (3) sedimentary, mainly flysch type units; (4) intrusive and intermediate and high-grade metamorphic rocks of crustal Alpine units; (5) Miocene to Holocene sedimentary autochthonous units (from Sorriso-Valvo, 1993).
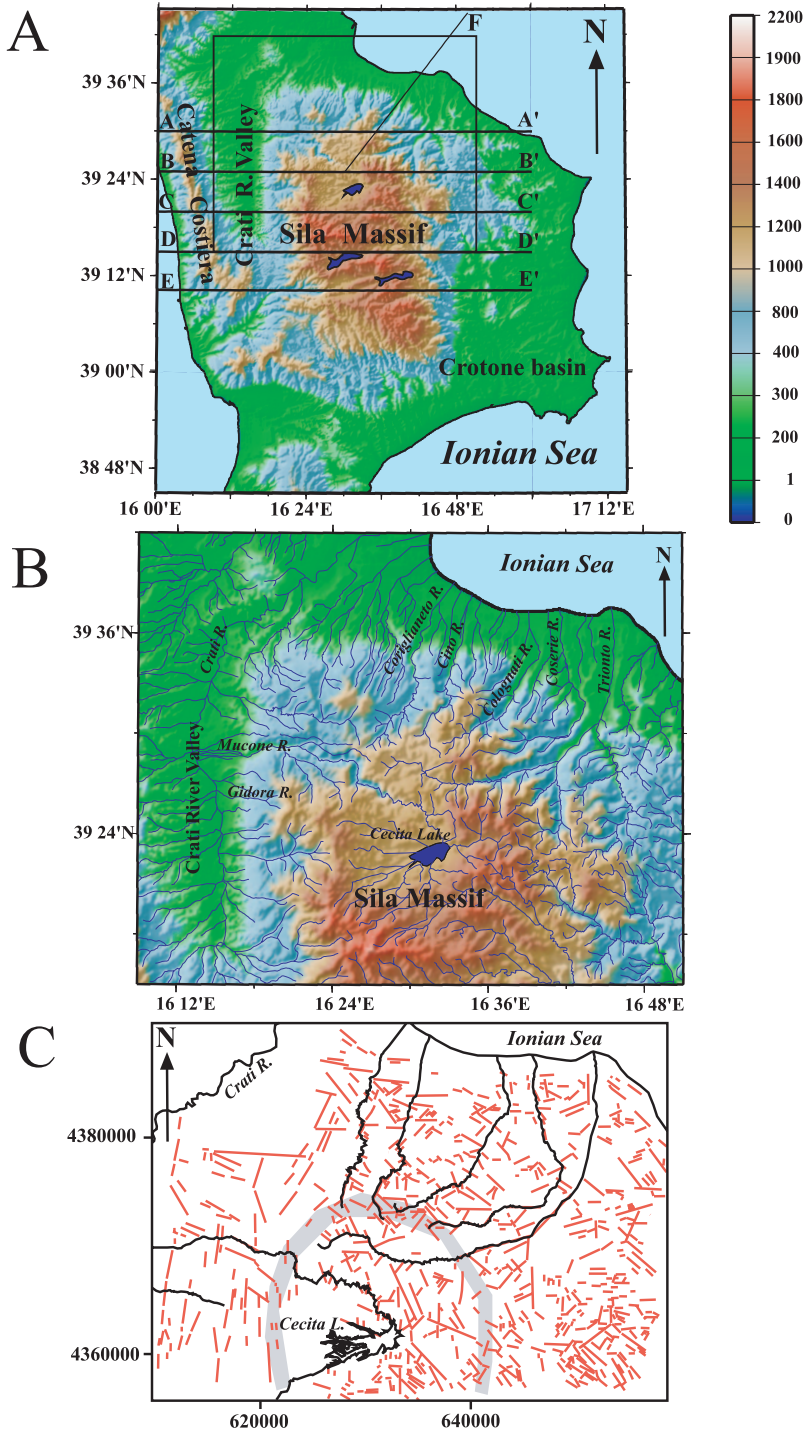
Fig. 2. (A) Digital shaded topographic map of the regional topographic setting of northern Calabria showing the entire Sila Massif separated from Catena Costiera by the Crati River Valley; the location of the study area and of the cross-section illustrated in figs. 7 and 8 are reported. (B) Detail of (A) showing the northern portion of La Sila and the streams investigated in this study. (C) Map showing the major mapped lineaments in the context of the investigated streams and the location of the plateau rim (gray shaded area).

(Magnaghi-Vavilov basin, 4-5 Ma; Marsili basin, 2 Ma). Backarc basin sediments record the progressive east to southeastward migration of the locus of extension (Sartori, 1989; Faccenna and others, 1997) (fig. 1A) consistent with continued growth, eastward migration, and shortening in the forearc (Malinverno and Ryan, 1986; Royden and others, 1987; Mostardini and Merlini, 1988; Patacca and others, 1990; Bertotti and others, 1997; Gueguen and others, 1998; Amato and Cinque, 1999; Cavinato and De Celles, 1999).

The Apennines, including Calabria, are characterized by local shortening in the foreland to forearc transition, and extension through the arc and into the backarc (Royden and others, 1987; Patacca and Scandone, 1989; Patacca and others, 1990; Lavecchia and others, 1994; Negredo and others, 1999). Calabria represent the emergent forearc high; however the data constraining the precise topographic emergence history and unroofing of Calabria, indeed of all the Apennines remains equivocal. Forearc and backarc basins are filled with late Miocene to early Pliocene continental siliciclastics of Hercynian and Mesozoic-Cenozoic mixed carbonate-siliciclastic provenance (Calamita and others, 1999; Cavinato and De Celles, 1999). A geomorphic record of this early emergence and erosion of the chain may be recorded by low-relief upland surfaces in several high-standing parts of the Apennines (Dramis and others, 1990; Dramis, 1992; Amato and Cinque, 1999; Ascione and Cinque, 1999; Calamita and others, 1999).

During the late Pliocene to late early Pleistocene, a decrease in the rate of the eastward migration of the Apennines (Mantovani and others, 1996) and a minor change in the backarc extension axis are temporally coincident with an increase of regional topographic emergence of the range (Hippolyte and others, 1994). Although there is little agreement on the mechanisms for the accelerated, recent emergence of the range, there is mounting geologic evidence to support significant rock uplift of the entire Apennine chain by the middle Pleistocene (Ciaranfi and others, 1983; Brancaccio and others, 1984; Colella and others, 1987; Dramis, 1992; Moretti, 1993; Tortorici and others, 1995; Moretti and Guerra, 1997; Amato and Cinque, 1999; Ascione and Cinque, 1999; Calamita and others, 1999; Feroni and others, 2001).

Our study focuses on the Sila Plateau of central Calabria which lies in the uplifted forearc and is underlain by crystalline, continental, and oceanic metamorphic rocks ("Complesso Ofiolitico", Auct.) thrust over Mesozoic carbonates and flysch (Ogniben, 1973; Amodio-Morelli and others, 1976; Dietrich, 1976; Lanzafame and others, 1979; Critelli, 1990) (fig. 1B). The metamorphic and crystalline rocks are generally deeply weathered to a saprolite several meters to a few tens of meters deep (Le Pera and Sorriso-Valvo, 2000). Meso-scale fractures and faults impart a rectilinear ruggedness to the topography and locally control drainage patterns (Molin, ms, 2001). La Sila is a plateau with a rolling upland lying about 1500 m above sea level, a gently depressed interior, and gently raised edges. A natural lake in the vicinity of the modern Cecita Lake reservoir occupied the center of the plateau at times during the Pleistocene (Henderson, 1970; Dramis and others, 1990; Galli and Bosi, 2003).

Sila is separated from the surrounding landscape by large dip- and oblique-slip normal faults that form steep escarpments with distinct triangular facets. The northern and northeastern flanks are marked by NW–SE, WNW–ESE and N-S trending faults (Ciaranfi and others, 1983; Moussat and others, 1986; Knott and Turco, 1991; Sorriso-Valvo, 1993) whereas the western flank is defined by a seismogenic segmented range-front fault zone separating Sila from the Crati Valley (Lanzafame and Tortorici, 1981; Tortorici and others, 1995). This range front fault system defines one of the most active seismic regions in the Mediterranean (Ghisetti and Vezzani, 1982; Cristofolini and others, 1985; Tortorici and others, 1995; Monaco and Tortorici, 2000). The eastern flank is delimited by N-S trending extensional faults that are the northernmost

end of a system that separates the southern portion of Sila Massif from the Crotone basin (Moretti, 1993). The low-standing extensional basins surrounding Sila are filled by several upper Tortonian–Holocene depositional sequences composed of poorly consolidated marine and fluvial conglomerate, sand, and clay (Vezzani, 1968; Ogniben, 1973; Lanzafame and Tortorici, 1981; Colella and others, 1987; Critelli, 1990; Colella, 1995; Tortorici and others, 1995).

Erosion, and presumably rock uplift of Sila is broadly constrained by thermochronologic and geomorphic data. Apatite fission track thermochronology (AFT) indicates rapid cooling of the crystalline basement rocks between ~35 Ma and ~15 Ma (Thomson, 1994). This cooling has been interpreted as the result of Oligocene-Miocene syn- and late-orogenic crustal extension as well as an increased rate of subaerial erosion (Thomson, 1994). Quaternary rates of rock and surface uplift have been approximated by the amount of fluvial incision below dated stratigraphic horizons generated at or near sea level including fluvial and marine terraces (Colella and others, 1987; Gliozzi, ms, 1988; Palmentola and others, 1990; Carobene and Dai Prà, 1990; Cucci and Cinti, 1998; Molin, ms, 2001; Molin and others, 2002). Rock uplift rates vary locally because of a complex interaction between the deformation apportioned to individual active faults and a longer-wavelength deformation of the entire Calabrian forearc. Several mechanisms have been proposed to drive the longer-wavelength deformation including post-orogenic isostatic rise (Ogniben, 1973; van Dijk and Scheepers, 1995), crustal arching caused by late orogenic regional undulation (Wezel, 1986), doming of the Tyrrhenian rift flank (Bousquet, 1973), oroclinal bending (Ghisetti, 1979), dynamic response to tectonic style changes in the subduction zone (Giunchi and others, 1996), asthenospheric upwelling in the wake of subducting slab rollback (Moretti, 1993; Moretti and Guerra, 1997; Calamita and others, 1999), slab detachment (Carminati and others, 1998; Calamita and others, 1999; Wortel and Spakman, 2000), and rebound of the forearc following delamination of the subducting slab (Gvirtzman and Nur, 1999, 2001).

METHODS

This study analyzes landforms at a variety of scales designed to characterize both local and regional tectonic processes. The two primary data sources are paper IGMI (Italian Geographic Military Institute) topographic maps of Calabria at scales of 1:100,000 and 1:25,000 and the digital elevation model of Italy provided by the Italian Geologic Survey (fig. 2A and B). The DEM has a pixel resolution of 7.5 seconds latitude and 10 seconds longitude digitized from 1:25,000 scale topographic maps by IGMI. We further processed the DEM data to produce a grid composed of cells with equal dimensions of 250 m. A newly released 90 m resolution DEM derived from the SRTM data is used for river longitudinal profile analysis. These topographic data are complimented by field investigations performed by the first author from 1997-2001 and reconnaissance field studies by all authors in the summer of 2000.

Topography and Envelope, Subenvelope, and Residual Relief Maps

We have generated several DEMs of the study area by digitizing points on 1:100,000 scale IGMI topographic maps and, following the general technique outlined in Keller and Pinter (1996), to construct enveloping surfaces of that topography. Specifically, the intersections of consecutive 200 m interval contours with stream channels and major interfluves have been digitized, interpolated, and rendered into a DEM grid with 100 m cell spacing using the publicly available GMT (Generic Mapping Tools) software. The raw DEM was smoothed in the frequency domain using a Fast Fourier Transform (FFT) low-pass filter to remove all wavelengths smaller than 3 km and cosine tapers all wavelengths between 3 and 5 km. The 3 km spatial domain wavelength was chosen because it represents the average main valley spacing resolvable

by our digitizing and the cosine tapering helps insure that no numeric artifacts are introduced during the filtering process. From this smoothed, mean topographic surface we extract a surface corresponding to the general form of the peak elevations, called the envelope and a surface corresponding to the general configuration of valley bottoms called the subenvelope. The relative relief between the envelope and subenvelope, called the residual, is generated by subtracting the two enveloping surfaces. The residual reveals where the landscape is deeply incised in a way that is not immediately obvious from the smooth topography alone. In the active tectonic landscape, regions of anomalously high relief are commonly coincident with regions of active stream incision in response to rock uplift.

Stream Long Profiles and the SL Index

A stream longitudinal profile (long profile) is a plot of channel or valley length with respect to channel or valley elevation above sea level (fig. 3A). The local tectonic deformation we wish to investigate can be accommodated by adjustments in channel sinuosity (Schumm and others, 1987, 2000), so we use the valley long profiles because they are a better measure of tectonically-induced gradient changes than the channel long profiles. We have generated long profiles for streams in Calabria using a Lasico electro-mechanical digitizer and 1:25,000 IGMI topographic maps as well as extracting the profiles directly from the DEMs. We digitized the UTM locations of consecutive 25 m interval contour lines off the paper maps and sampled the DEMs at 100 m horizontal intervals (fig. 3A). Long profiles of alluvial channels and many bedrock or mixed-bedrock-alluvial channels typically are concave-up, a shape traditionally equated with a graded, equilibrium profile (Mackin, 1948). The concave-up shape arises, in part, from the fact that as peak annual discharge increases and grain size decreases downstream, lower gradients are needed to both transport the channel alluvium (Leopold and others, 1964), and incise into bedrock (Pazzaglia and others, 1998). Deviations from a smooth, concave-up form may indicate that the fluvial system is in a transient state of adjustment to a base level, tectonic, climatic, or rock-type perturbation. In particular, convex segments called knickpoints or knickzones depending upon their length compared to the total stream length, can be specifically investigated to evaluate their coincidence with tectonic perturbations at scales ranging from massif-wide doming, to offset across local faults.

To quantify the general shape of stream long profiles, we have measured the profile's concavity (the rate of change of profile curvature) by two methods (fig. 3B). In the first method, concavity (σ) is calculated as the normalized area under the stream long profile (A_p) with respect to the area of a right triangle (A_{tr}) where the hypotenuse connects the divide to the mouth of the long profile (Wells and others, 1988; Demoulin, 1998):

$$\sigma = 1 - (A_p/A_{tr}) \tag{1}$$

The second method takes advantage of the well known power law relationship between channel gradient and upstream drainage area,

$$S = k_s A^{-\theta} \tag{2}$$

where θ ranges from ~0.2 to 1.0 (Hack, 1957; Flint, 1974; Tarboton and others, 1989; Snyder and others, 2000; Kirby and Whipple, 2001). In equation (2) long profile concavity is θ and the profile steepness is k_s, the slope and y-intercept respectively of a line regressed through a log-log plot of channel slope and drainage basin area (inset fig. 3A). The variables for channel steepness and concavity are important characteristics of the long profile to measure because the erosion rate of a predominantly detachment-limited, perennial channel is commonly modeled as being proportional
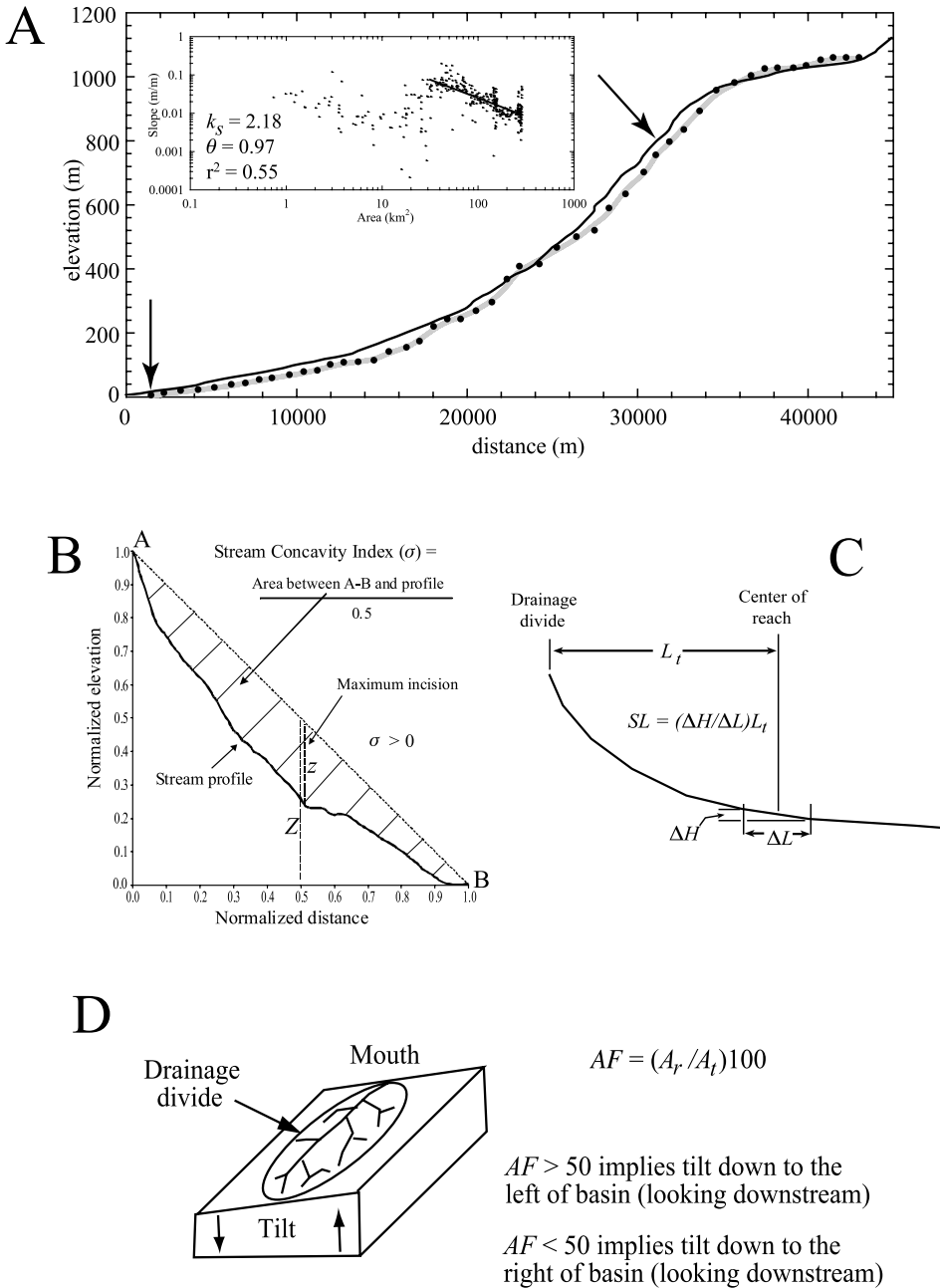
Fig. 3. (A) Example of a valley long profile (for location of Trionto River see figure 2B). The solid black line was obtained by digitizing paper maps, the data points were extracted from the 250 m DEM, and the solid gray line is a smooth version of the data extracted from the same DEM. The inset graph is a plot of Trionto channel gradient as a function of drainage area. Values for concavity (θ) and steepness (k_s) are obtained by regression through the lower part of these data, between the arrows, that represent dominantly bedrock channel fluvial processes on the flanks of Sila. (B) Calculation of concavity (σ) using a geometric ratio on a normalized profile (modified from B. Zaprowski, F. J. Pazzaglia, and E. B. Evenson, 2004, unpublished data). (C) Example of how the *SL* index is generated for a reach of a stream profile (modified from Hack, 1973). (D) Example of the calculation for drainage basin asymmetry (modified from Keller and Pinter, 1996).

to a power-law function of basal shear stress (Howard and Kerby, 1983; Snyder and others, 2000). Assuming steady, uniform flow, the conservation of mass (water), a linear (or nearly linear) relationship between discharge and drainage area, and a channel width that grows as a function of the square root of the discharge, the erosion (*E*) law for bedrock channels becomes

$$E = KA^m S^n \qquad (3)$$

where m and n are real, positive exponents determined by the channel erosion process and *K* is a proportionality factor incorporating climate and rock-type (see Snyder and others, 2000 for a complete derivation of equation 3). For the case where the long profile is perfectly graded, the rate of change of elevation along the profile (*dz/dt*) is zero which requires that channel erosion is uniform and equal to the rate of rock uplift (*U*),

$$dz/dt = 0 = U - E = U - KA^m S^n \qquad (4)$$

Equation (4) can be rearranged to solve for channel slope as a function of drainage basin area,

$$S = (U/K)^{1/n} A^{-m/n} \qquad (5)$$

an expression with the same general form of equation (2) where profile steepness (*k_s*) is analogous to *(U/K)^{1/n}* and *m/n* is analogous to *θ*. Equation (5) predicts a linear relationship between log *S* and log *A* where the *m/n* parameter is 0.5 when erosion is proportional to basal shear stress (Whipple and Tucker, 1999). The symmetry between equations (2) and (5) allows for a direct comparison between real stream profile concavities extracted from long profiles (*θ*) and the model-predicted concavity (*m/n*=0.5) assuming perfectly graded conditions. Concavity on a slope-area plot is roughly correlative to the exponent in "Hack's Law" (Hack, 1957) and is influenced by watershed hydrology. Profile steepness is similar to the stream-gradient index (Hack, 1973) and is influenced by the rate of rock uplift as well as rock-type. We model profile steepness for the graded concavity value of 0.5 as well as the measured mean concavity of Calabrian streams. Both *θ* and *σ* allow for direct comparison of basins of different size. The slope-area plot method has the added advantage for removing any effects of basin shape on the resulting long profile.

The spatial distribution and potential origin of knickpoints are highlighted by the stream-gradient (*SL*) index (Hack, 1973) (fig. 3C):

$$SL = (\Delta H/\Delta L)L_t, \qquad (6)$$

where *H* is elevation, *L* is length of stream reach, and *L_t* is the total stream length measured from the divide to the midpoint of the stream reach under investigation. Normalizing with respect to *L_t* allows for direct comparisons between small drainages that typically have steep long profiles and larger drainages that have more gentle long profiles. The *SL* index is particularly sensitive to knickpoints that may be the result of base level fall, a rock-type change, and/or active tectonics. In our study area, the relatively uniform rock-type underlying La Sila, locations of mapped faults, and proximity to sea level with known eustatic changes helps us interpret long profile data in an active tectonic context.

Drainage Basin Asymmetry

General tilt of the landscape to both local and regional tectonic deformation may be recorded in the planimetric view of drainage basin shape if the basin is favorably oriented with respect to the axis of tilting (fig. 3D). We have utilized the methodology

presented by Gardner and others (1987) in the calculation of drainage basin asymmetry (AF),

$$AF = (A_r/A_t)100 \qquad (7)$$

where AF is the asymmetry factor, A_r is the drainage area on the downstream right of the main drainage line and A_t is the total drainage area. When AF is greater than 50, the channel has shifted towards the downstream left side of the drainage basin. A value less than 50 indicates that the channel has shifted towards the downstream right side of the drainage basin.

It is important to restrict direct comparisons of AF to drainages of roughly the same size. We ordered the drainage network on 1:100,000 scale maps following the Strahler (1957) methodology and extracted the AF from third and fourth-order drainages only. The direction and magnitude of the AF can then be plotted on a map as a vector.

Basin Shape and Hypsometry

The drainage basin shape and the basin hypsometry are parameters that can yield information about the relative drainage efficiency in a watershed. Hypsometry is influenced by basin size, rock-type (Hurtrez and Lucazeau, 1999), and whether the basin is experiencing predominantly erosion or aggradation (Masek and others, 1994a). Willgoose and Hancock (1998) noted that hypsometry is dependent on basin shape and the planimetric form of the drainage network. Considering that the Sila drainages we studied are mostly underlain by the same rock-type, that Strahler (1952) ordering shows them to have similar drainage networks for similar area drained, and that all of them are incising, we feel that we can make meaningful hypsometric comparisons between basins. We calculate basin hypsometry with the hypsometric integral (Keller and Pinter, 1996 and references herein),

$$I = (h_{mean} - h_{min})/(h_{max} - h_{min}) \qquad (8)$$

where I is the hypsometric integral, and h_{max}, h_{min}, and h_{mean} are the maximum, the minimum, and the mean elevation respectively. The maximum and the minimum heights have been read directly from topographic maps. The mean elevation is obtained by randomly sampling at least 50 points on the map and then calculating the mean value. Results from sampling the topographic map are comparable to results from sampling the DEM.

Structural controls aside, in actively uplifting landscapes, youthful basins are commonly held to be relatively elongate with little of their area lowered to near base level. On the contrary, interbasin integration and elaboration as erosional processes equilibrate to, or exceed rates of rock uplift are relatively equally shaped and contain relatively little area high above base level. We have measured the degree of basin elongation using the elongation ratio (E_b) (Schumm, 1956):

$$E_b = \frac{2\sqrt{\dfrac{A_b}{\pi}}}{l_b} \qquad (9)$$

where A_b is the diameter of a circle of the same area as the drainage basin and l_b is basin length measured from its mouth to most distant point on the watershed limit. The closer the ratio approaches 1, the more the shape of the basin approaches a circle. In contrast, low values are consistent with narrow, elongate basin shape, commonly accompanied by high local relief and steep valley slopes.

Cross Profiles

The 250m DEM has been sampled at regular intervals of 0.01 degree (~850 m) of longitude to generate east-west and northeast-southwest oriented cross profiles (fig. 2A). These profiles have been used to construct topographic swaths, illustrating changes in relief and providing complimentary information to the topographic residual map. To produce the swath, elevations have been compiled and averaged for five adjacent cross profiles in an observation window with a length dimension equal to 1 degree of longitude and a width dimension equal to 5 minutes of latitude. Such a window width is about half as wide as the major drainage basins, and the size insures that the minimum and the maximum elevations of the river valleys and interfluves are captured.

DATA

General Drainage Pattern

The Sila interior is drained by two major streams, the Trionto and the Mucone rivers. The Trionto River traverses the north-eastern plateau edge and then flows northward to the Ionian Sea (fig. 2B). The Trionto basin is asymmetric as most of its tributaries enter from the east. The Mucone River is a hooked-shaped tributary of the Crati River that deeply incises the plateau's western flank. The Mucone River headwaters flow ENE, but the trunk channel changes direction abruptly to a NW-SE trend at the mouth of the Cecita reservoir. All other streams draining the Sila Massif either flow into Cecita Lake or are external to the plateau, failing to breach its flanks. The headwaters and medial portions of these external drainages are bedrock channels deeply incised into the massif flanks forming narrow valleys with very steep slopes. Where the streams reach a hilly piedmont located at the foot of the northern flank and the adjacent coastal plain, they undergo an abrupt transformation to wide, shallow, sediment-choked braided channels. Here the interfluves preserve several inset fluvial terraces that indicate, through their correlation to dated marine terraces, a rock uplift rate of 0.6 mm/yr in the last ~350,000 yr (Molin, ms, 2001).

Crati River tributaries, which deeply incise the western flank of Sila, have wide alluvial fans at their confluence with the Crati River. Modern and ancient fan deposits are particularly well preserved at the Mucone-Crati confluence. At least three inset, undated fan deposits with highly-modified treads lie between 100 and 300 m above the present floodplain (Molin, ms, 2001).

Stream Long Profiles

Seven stream long profiles (fig. 4) and their corresponding concavity and steepness are used to characterize tectonics and base level fall. Five long profiles (Corigli-aneto, Cino, Colognati, Coserie and Trionto rivers) are located along Sila's northern flank and flow directly into the Ionian Sea. The Mucone and Gidora rivers, in comparison, flow west as major tributaries to the Crati River. The streams are underlain by uniform rock type, that is Paleozoic granite and schist, except close to the base level, where they are underlain by upper Miocene-upper Pleistocene sedimentary rocks (figs. 1 and 2). Only the Colognati, Coserie and Trionto rivers cross significant reaches of contrasting rock-types, and we indicate these reaches on the long profiles (fig. 4). All streams are third or fourth order (Strahler) except for the Mucone and Trionto rivers that are both fifth order. All the analyzed long profiles show a general concave-up shape with local straight or convex reaches that generally correspond to faults but never to rock-type changes (fig. 4).

The Coriglianeto River long profile has a knickpoint at an elevation between 100 and 200 m, which coincides with a WNW-ESE extensional fault. Just upstream of this knickpoint, there is a straight segment that corresponds to a widening of the valley
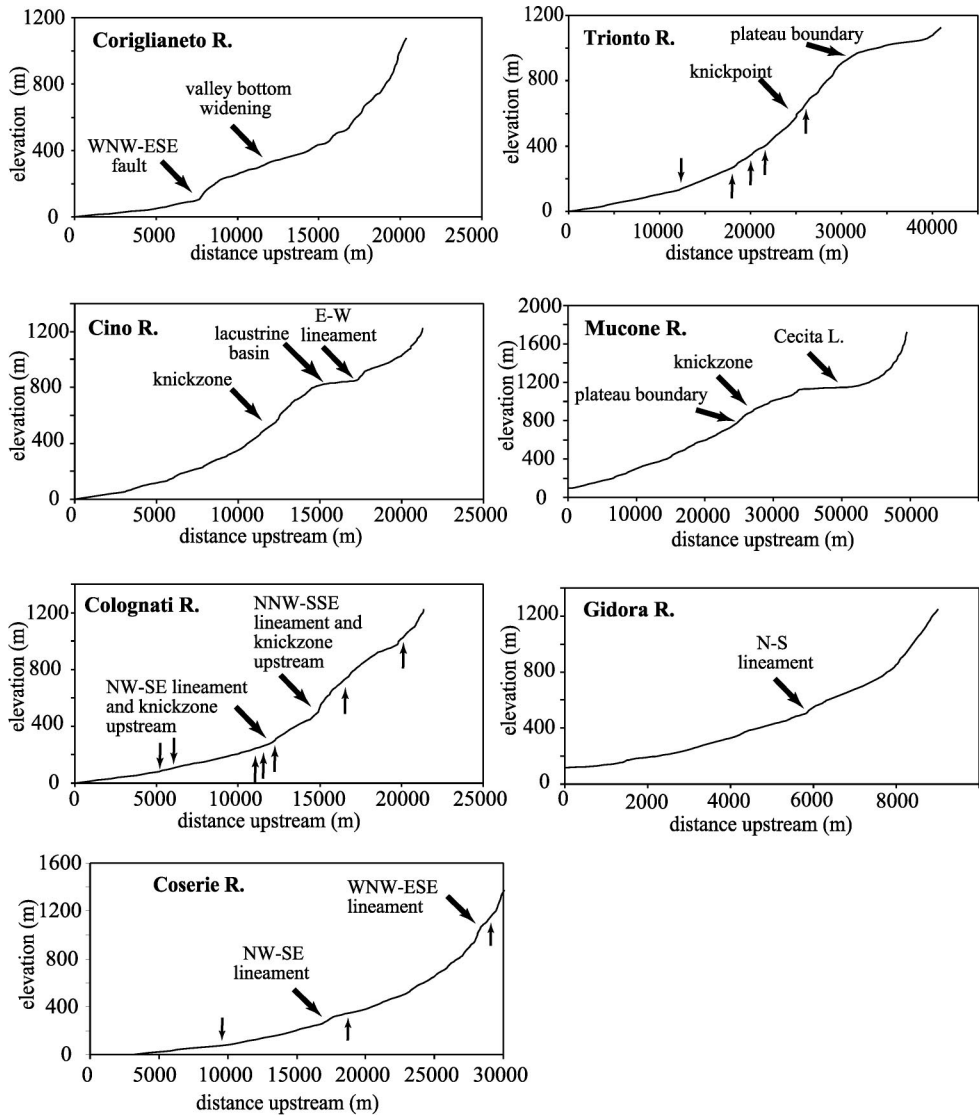
Fig. 4. Valley long profiles of the studied streams. Oblique arrows point to the main knickpoints and knickzones described in the text; vertical arrows indicate rock-type changes. For stream locations see figure 2B. Concavity and steepness of these profiles is found in table 1.

bottom and a braided channel pattern. Where the stream approaches the plateau edge, the profile becomes very steep with numerous small knickpoints.

The Cino River long profile is characterized by small steps below 400 m and a convex reach between 400 and 800 m. Through this reach, the channel passes from a braided pattern to a sinuous one and is entrenched in a narrow valley affected by faults. Further upstream, the profile flattens significantly along a reach corresponding to a NNE-SSW trending fault, parallel to the valley. This structure appears to control the

Drainage basin and long profile data

Stream	Concavity σ	Concavity $-\theta$	Raw k_s	modeled k_s $-\theta = 0.5$	modeled k_s $\theta = -0.74$	Elongation ratio	Hypsometric integral
Coriglianeto	0.44	−0.31	0.11	0.15	0.17	0.41	0.57
Cino	0.21	−0.5	0.23	0.23	0.46	0.40	0.56
Colognati	0.38	−1.16	2.14	0.34	0.7	0.46	0.47
Coserie	0.47	−0.76	0.35	0.18	0.32	0.45	0.37
Trionto	0.15	−0.97	2.17	0.25	0.73	0.39	0.50
Mucone	0.19	−0.89	3.17	0.44	1.53	0.41	0.42
Gidora	0.41	−0.57	0.52	0.54	1.12	0.45	0.52

location of a small basin where lacustrine and alluvial sediments are now exposed by river incision (Molin, ms, 2001). On the upstream side of this basin there is a knickpoint corresponding to an E-W trending lineament. Similarly, the adjacent Colognati River long profile is characterized by two main convex segments. The lower one is at an elevation of 300 to 450 m, and the larger concave segment is between 500 and 950 m. Both correspond to locations of a narrower valley and to a more sinuous channel.

The Coserie, Trionto, and Gidora long profiles generally have relatively simple concave-up shapes. On the Coserie River, this graded profile is interrupted by a knickpoint at ~250 to 300 m that corresponds to a NW-SE lineament. At this location the channel is entrenched in a narrow valley. A convex segment located between 1000 and 1200 m coincides with a WNW-ESE trending lineament. The Trionto River has a knickpoint at ~600 m followed by a convex reach extending to where the stream breaches the plateau edge at around 1000 m elevation. Here the profile decreases its gradient significantly. The knickpoint at ~600 m corresponds to a change from a braided channel to a narrow and entrenched one. Knickpoints on the Gidora River are close to mapped N-S lineaments.

The Mucone River long profile deviates significantly from a simple concave-up form. The profile is a composite of a lower almost straight channel with a knickzone coincident with the plateau rim, and an upper distinctly concave up channel upstream of the dam of Cecita Lake. It is this upper concavity that distinguishes the Mucone profile from the Trionto profile, the only other river to have breached the plateau rim.

The Mucone, Trionto, and Colognati channels have the most convex profiles, as measured by both the σ and θ concavity metrics (table 1). These profiles are also the steepest, as measured by the raw k_s values (table 1). The composite nature of the long profiles (fig. 4) makes it difficult to find a single regression through slope-area data (inset, fig. 3A). We have uniformly regressed through the data where basin area grows to larger than 20 km^2 and slope and area negatively covary. This captures the concavity and steepness of the lower portions of the profile (arrows in fig. 1A) and allows for direct comparison of all the rivers. The Mucone, Trionto, and Colognati channels continue to have the steepest profiles when concavity is modeled at the graded, equilibrium value of 0.5 and the average concavity value of the seven profiles of 0.74. The Gidora river profile also shows steep modeled k_s values, but this river is significantly smaller than the other six, and there are fewer data constraining the slope-area regression.

In summary, the smaller, external drainage streams like the Cino, Coserie, and Corigliamento show knickpoints and local convexities corresponding to lineaments or faults. Knickpoints are less evident on the larger Mucone and the Trionto rivers, but these profiles are the steepest and least concave. In contrast to concavity and steepness, there are only small variations and no discernable trends in both elongation ratio and hypsometric integral (table 1). Sila drainages are elongate and have relatively high hypsometric integrals. Both metrics are consistent with steep, actively incising streams.

Regional Topographic Metrics

Five different renderings of the Calabrian topography help visualize the distribution of relief in this landscape. The smoothed topography (fig. 5A) captures several length scales of valley spacing and depth including the elevated rim of the plateau. This rim is locally absent in the northwest where the Mucone River breaches the plateau edge and the Corigianeto and Trionto rivers head.

The envelope surface (fig. 5B) is draped across the ridgelines of figure 5A, and shows how the deeper incision of some drainages (Corigianeto, Trionto and Mucone rivers) influence the maximum topography pattern. Moreover, the envelope map shows the N-S, WNW-ESE, and NW-SE escarpments coincident with faults and lineaments (fig. 2A), defining the Sila Massif's western, northern and eastern boundaries respectively.

The subenvelope surface (fig. 5C) is stretched across the valley bottoms and mimics, to a first order, the local base level to which streams are lowering. The residual relief map (fig. 5D) clearly shows the low relief plateau interior and a higher relief plateau rim. In addition, there are some high relief features not readily apparent on the other maps. For example, the northeastern flank of the plateau is marked by a NNW-SSE trending residual high. First suggested by Cliff Ollier and Francesco Dramis for a zone of particularly deeply incised streams, we herein refer to this feature as the OD-ridge. This ridge appears as knickpoints or broader convexities in the longitudinal profiles of major streams that traverse it (fig. 4). The Corigianeto River long profile, in particular, shows a knickpoint at an elevation of 200 to 400 m coincident with the ridge.

A contoured plot of *SL* indices (fig. 6A) shows that there are two regions where the stream gradients are anomalously steep. One is along the Mucone River that corresponds to the deeply incised, straight segment of its long profile downstream of Cecita Lake. The highest *SL* index values lie just upstream of the plateau edge corresponds to a convexity in the long profile of the Mucone River (fig. 4). The other high *SL* index area is located in the northeastern Sila Massif flank and shows a NW-SE trending distribution that is coincident with the OD-ridge (fig. 6B). The highest values correspond to where mapped NW-SE faults cross the Cino River between 550 to 650 m elevation.

The calculated drainage basin asymmetry factors (*AF*) indicate there is a more or less equal distribution of the number of watersheds with maximum area on the downstream right and left of the trunk channel, but the watersheds are not spatially distributed uniformly. We note two general trends of basin asymmetry. The western flank of Sila has a majority of its watersheds that tilt to the north (fig. 6C). The northern flank of Sila has a distribution of basins tilting radially away from the aforementioned OD-ridge.

Cross Profiles and Mapped Geology

Six cross sections (figs. 2A and 7) provide a common frame of reference for comparing data extracted from the topographic analysis to geologic data obtained largely in the field. The cross sections show two main areas of high-standing topography, the Catena Costiera and the Sila Massif, separated by the Crati River Valley. The
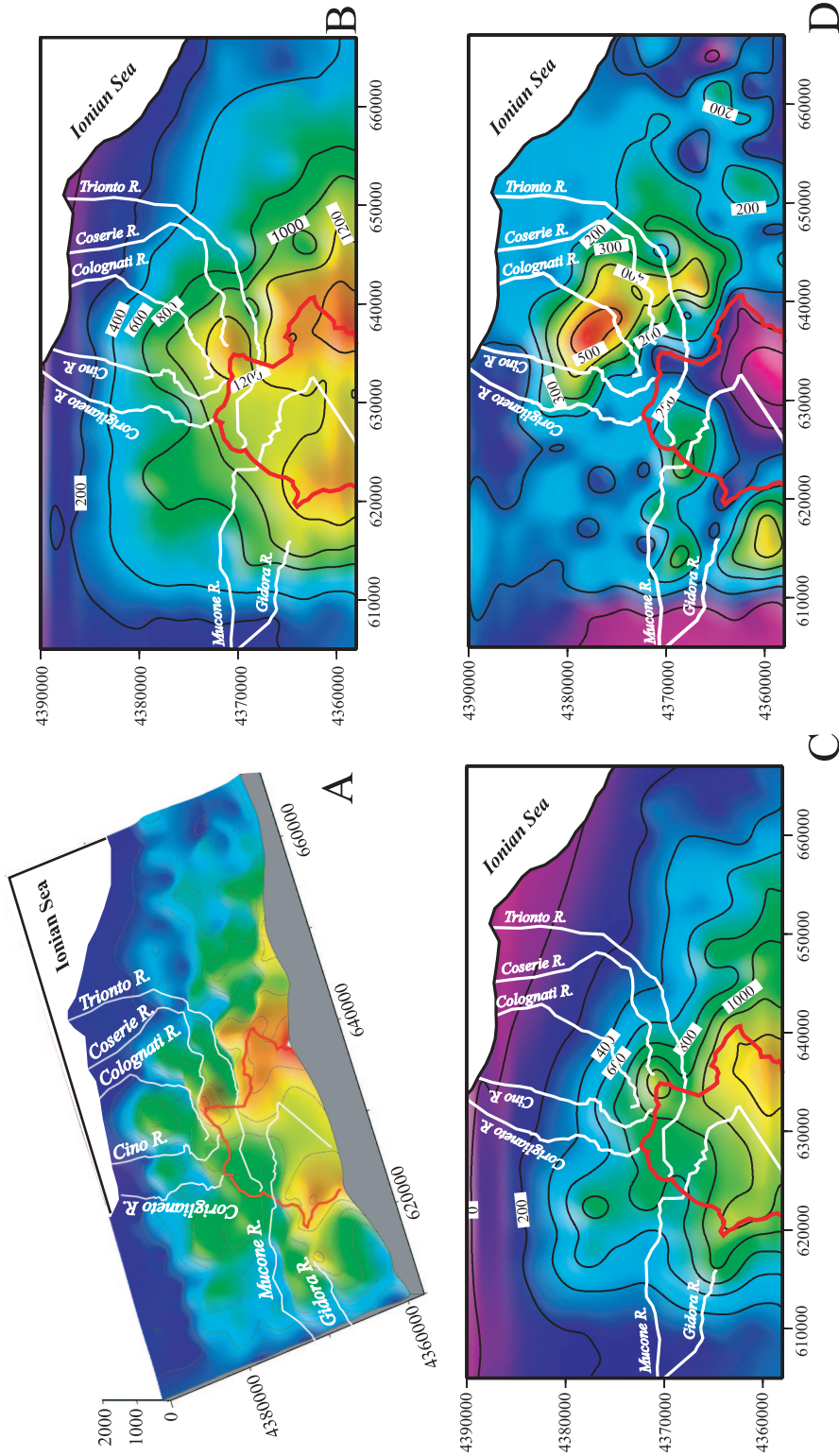
Fig. 5. Topographic maps of the northern part of the Sila Plateau. Warm colors indicate high elevation, cool colors indicate low elevations. The red polygon approximates the outline of the plateau edge as defined on paper 1:100,000 scale maps. (A) 3-D view of the smoothed topography of the northern sector of the Sila Massif. This DEM has been generated by a dataset of elevation points digitized on main mountain peaks, interfluves, and valley bottoms. (B) Envelope surface, that shows the general elevation of mountain peaks and intervening interfluves. (C) Subenvelope surface, showing the general configuration of valley bottoms through the connection of points digitized on stream channels. (D) Residual map, generated subtracting arithmetically the subenvelope from the envelope.
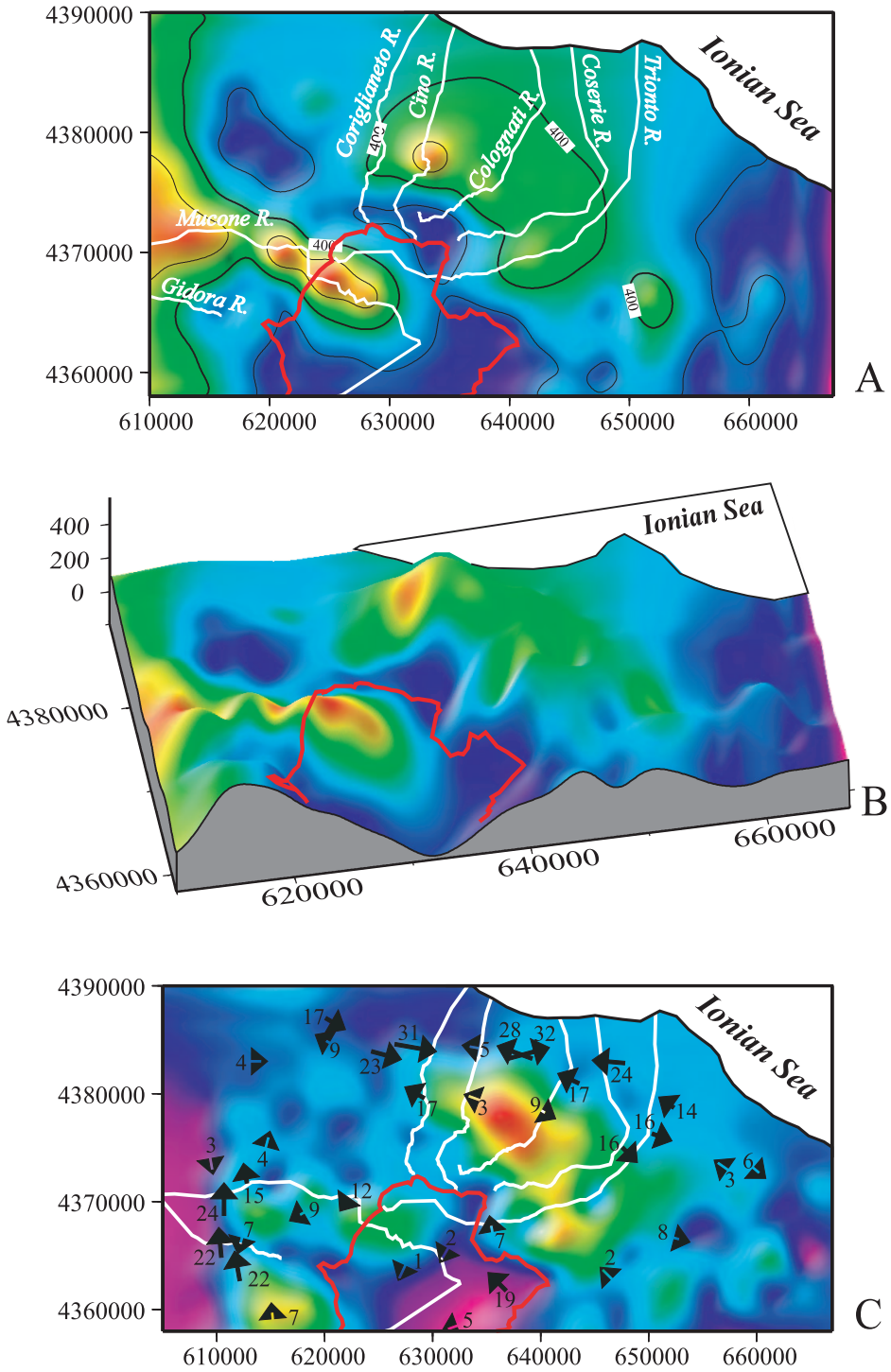
Fig. 6. (A) Contour map showing the spatial variations of the *SL* index obtained by calculating the slope steepness variations with respect to the stream head. Warm colors are high *SL* values, cool colors are low *SL* values. (B) Draping the *SL* index intensity colors on a 3-D view of the residual topography to point out the

BB′, BF, and CC′ profiles in particular show the elevated plateau rim, and low-relief interior. In the BB′ profile the eastern rim, which generally coincides with mapped NW-SE trending, southwest-dipping extensional faults located east of the Cecita Lake, reaches higher elevations than the western rim. In all of the profiles the western flank of the Sila Massif is very steep and coincident with the active west-dipping faults that define the Crati River Valley.

In the AA′, BB′, and BF profiles, the rugged topography of the eastern flank of the Sila Massif coincides with the OD-ridge (fig. 5D). Profiles BB′, CC′, DD′, and EE′ are deeply incised in the eastern flank of Sila corresponding to mapped N-S lineaments and the northward projection of extensional faults mapped south of the study area (Moretti, 1993; Moretti and Guerra, 1997). Degree of dissection by both streams and faults increases to the south (fig. 7, profiles DD′ and EE′); however, the plateau interior and its elevation rim are still discernable through a topographic envelope fit to accordant summits.

Two swath profiles (fig. 8) have been constructed between cross sections of figure 7. A northern swath lies between AA′ and BB′ profiles (fig. 8A), whereas the southern swath lies between the BB′ and CC′ profiles (fig. 8B). In the northern swath (fig. 8A), the maximum elevation has a general trend that is not mirrored in the average and minimum elevations profile. The anticorrelation between the maximum elevations and minimum elevations is consistent with where the Mucone and Trionto rivers breach and erode into the plateau edge. Relief in this swath is attributed to incision of the Mucone River in the western flank and by stream incision of the OD-ridge to the east. In this way, the plateau rim is not only defined by its elevation, but also by its increased relief. In contrast, the maximum, minimum and average elevations of the Catena Costiera in the western part of this swath are quite similar, but the relief remains high.

In the southern swath (fig. 8B), the plateau and its elevated rim are all mirrored by the maximum, the minimum, and the average elevations. Coincidentally, there are no streams that breach the plateau edge at the latitude of the southern swath. Here the residual relief is not as high as in the northern profile. Catena Costiera appears similarly in the southern swath as it does in the northern swath.

Relief is not randomly distributed in the dissected portions of the Calabrian landscape. Rather, it tends to maintain a more or less constant value, which for these swath profiles is latitudinally dependent. In the northern swath (fig. 8A), maximum relief for both the Catena Costiera and Sila flanks lies between 700 to 800 m. In the southern swath, the maximum relief is approximately 200 m lower (fig. 8B). The maximum relief is clearly not well correlated with either the width or with the average elevation of the topography. Similarly, little fluvial incision is indicated by the maximum, minimum and average elevations astride the western margin of the Sila Plateau despite the presence of an active fault. In contrast, there is far greater dissection of the eastern flank of the Sila Plateau where normal faults are also known to border the massif.

Flexural Model of the Sila Plateau

Elevation, relief, and long profile data all suggest a plateau rim that is being actively uplifted with respect to its interior. We investigate a possible flexural origin for

---

high correlation between local relief and *SL* index. (C) Drainage asymmetry map where the plotted arrows indicate the direction of the asymmetry as well as its magnitude which is shown by the length of the arrow. The arrows are located at about the middle of the drainage area with the end on the trunk channel, and are projected on the residual topography map. In all maps the red polygon approximates the outline of the plateau edge as defined on paper 1:100,000 scale maps.
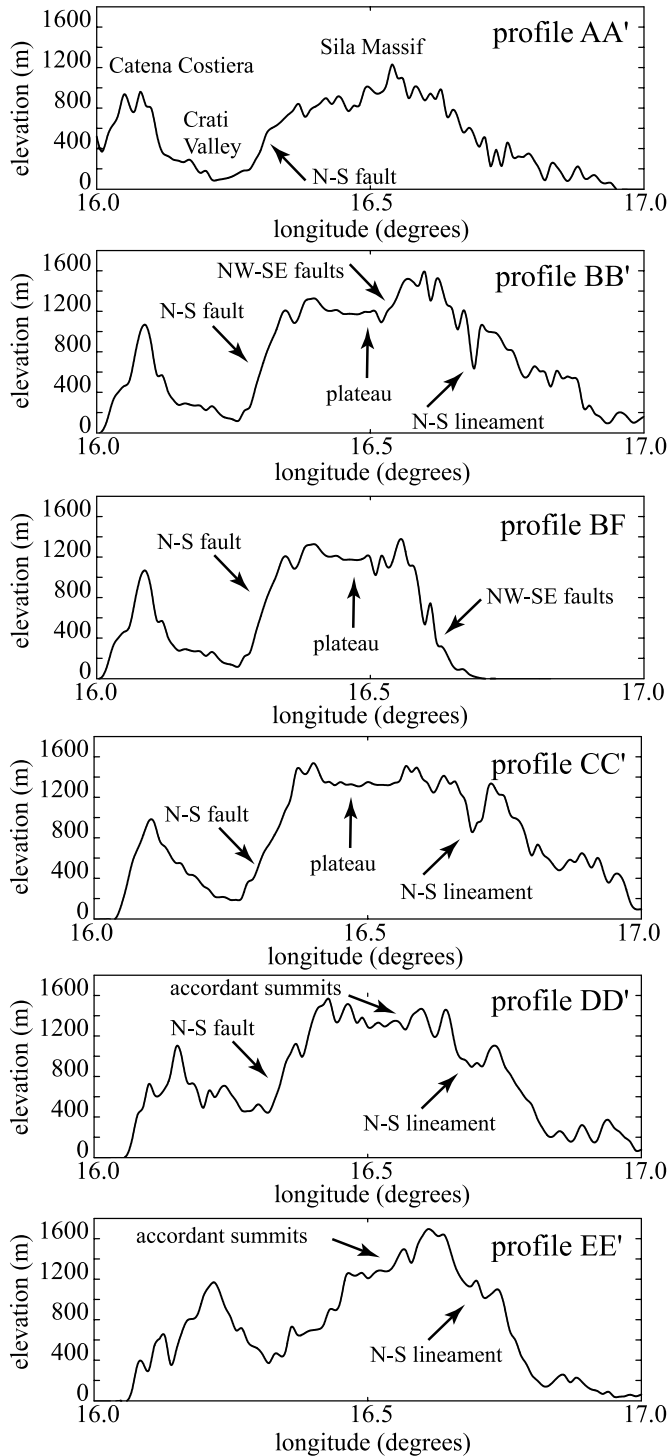
Fig. 7. Cross sections across northern Calabria (for location see figure 2A) that sample the topography at regular 0.01 degree or 860 m intervals. All the sections are E-W trending, except for BF that consists of two segments, which are oriented E-W and SW-NE. All these sections show the Catena Costiera westward and the Sila Massif eastward, separated by the valley of the Crati River.
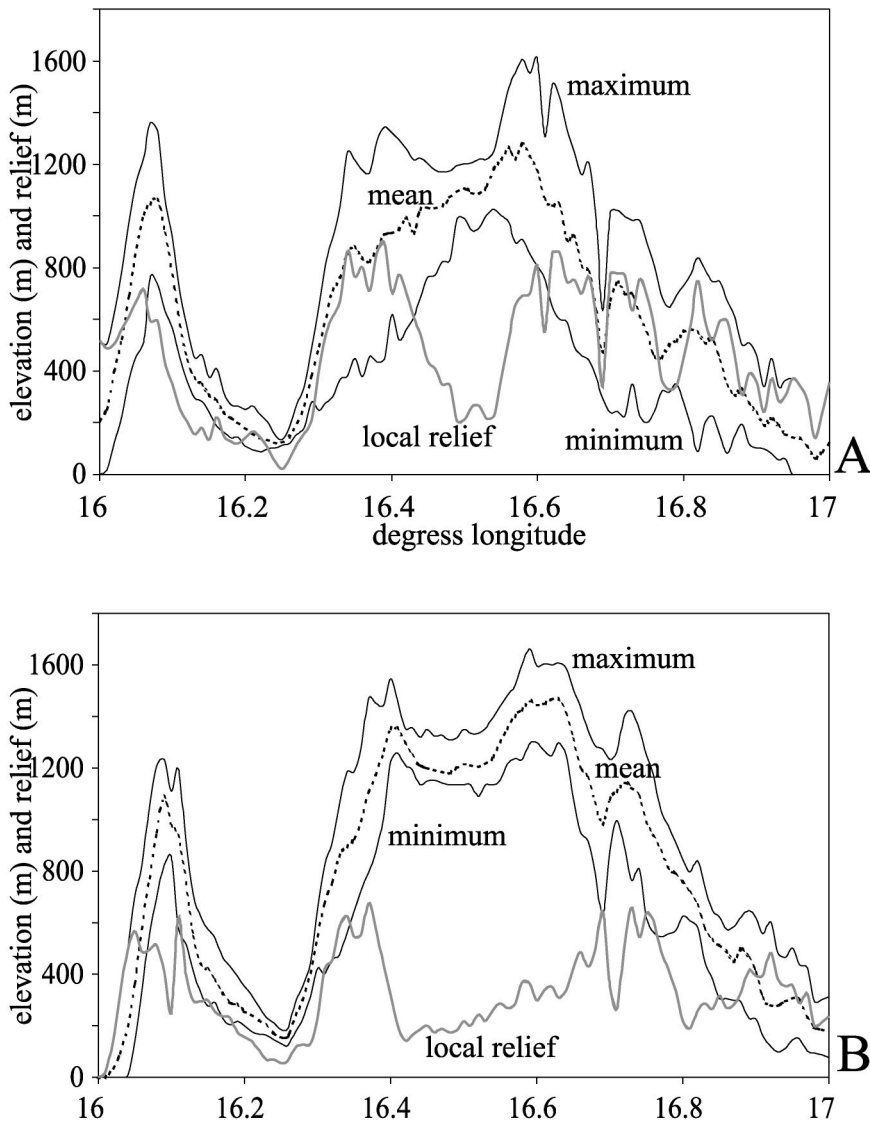
Fig. 8. Minimum, maximum, and average elevation extracted from a suite of adjacent cross profiles contained within a window of about 700 km^2 (1° of longitude for 5′ of latitude) areas defined by the traces of (A) AA′ and BB′ profiles and (B) BB′ and CC′ profiles of figures 2. The local relief is computed by arithmetical subtraction between maximum and minimum elevation.

this uplift. Our analysis is motivated by similar studies in tectonically active areas which have demonstrated that tectonic unloading of a footwall can lead to its subsequent flexural uplift (Vening-Meinesz, 1950; Wernicke and Axen, 1988; Brown and Phillips, 1999; Roy and others, 1999). In our case, we note that the flanks of the Sila Massif are bound by high-angle normal faults. The west-dipping Crati Valley faults and north-
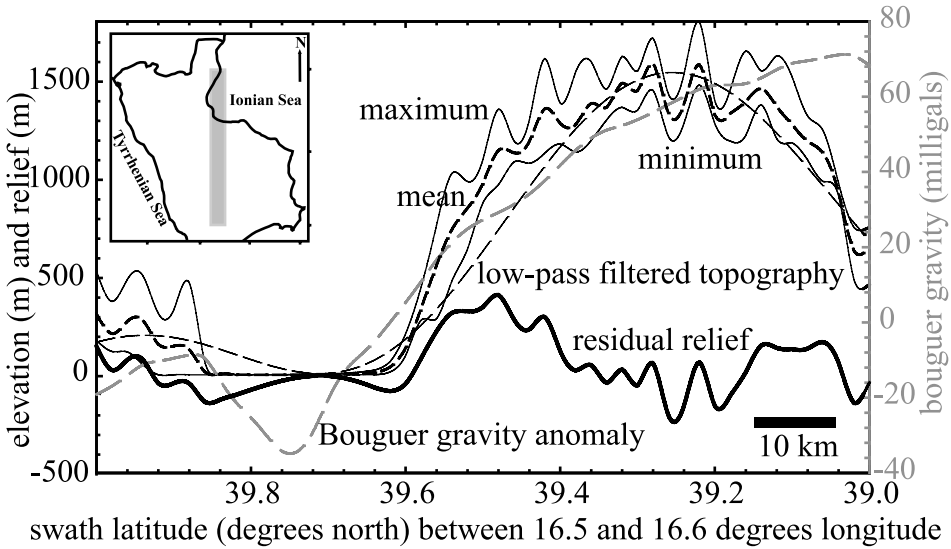
Fig. 9. North-south oriented swath profile illustrating minimum and maximum elevations (solid, thin black lines), average elevation (dashed, thick black line), low-pass filtered topographic elevation where all topographic length scales less than 50 km have been removed (thin, dashed black line), Bouguer gravity anomaly (thick, dashed, gray line), and residual topography produced from subtracting average topography from the filtered topography (thick, solid black line).

dipping Ionian margin faults have essentially unloaded the plateau edge as the crust has been extended. The analysis is designed to isolate the effects of shallow loads like basin infill and plateau margin erosion that are compensated regionally by lithospheric flexure, from the effects of deep, broad loads like the subducting slab (Royden and others, 1987) that for our operational scale, are compensated locally (Airy isostasy). The goal here is not to try to completely explain the elevation of the Sila rim with a flexural mechanism. Rather, we will first attempt to remove the effects of long-wavelength uplift of the massif by filtering the topography and conducting our analysis on the residual topography that captures the appropriate length scale of flexural deformation.

The east-west swath profile (fig. 8B) and a complimentary north-south swath profile (fig. 9) are well situated for the flexural model. To isolate the relatively short-wavelength components of the topography most sensitive to the flexural length scale, we first smoothed the DEM provided by the Italian Geological Survey using a low-pass filter to remove all wavelengths smaller that 50 km, and to cosine taper all wavelengths between 50 and 60 km. This low-pass filtered topography is analogous to an envelope map (fig. 5C), except that it is fit to the mean, rather than minimum or maximum elevations. Our choice to use 50 km as the appropriate cut-off wavelength for the low-pass filter was determined by matching the low-pass filtered topography to the wavelength of the Bouguer gravity anomaly which is an independent measure of how the long wavelength components of the topography are compensated at crustal length scales. Then we obtain a swath profile of this low-pass filtered topography coincident with our east-west and north-south oriented topographic swaths. Subtracting the filtered topography from the DEM topography results in the desired residual topography (fig. 9). The topographic residual profile has an amplitude less than the raw topography (see BB' profile in fig. 7), and is corrected to a common datum. It clearly shows the relatively high standing plateau rim and the general decay of the

topography toward the plateau interior. We fit the flexural model to this residual topography.

Any short-wavelength flexural topography attributed to footwall unloading is influenced by numerous considerations including the transmission of stress across the fault between the hanging wall and the footwall, dip of the fault, amount and density of basin infill, and thermal structure of the lithosphere (flexural rigidity). We do not have enough independent geologic data to tightly constrain all of these variables so we adopt a two-stage approach to the model. First, we adjust the load at the origin and the plate elastic thickness (flexural rigidity) and solve for the best flexural profile fit defined by a simple least squares fit, to the residual topography. Similar approaches have shown that elastic thickness can vary by a factor of two when the load and its precise location are treated as free parameters (Brown and Phillips, 1999), but it at least gives us a starting point for the range of acceptable rigidities. We subsequently attempt to reduce some of our free parameters by applying loads to the flexural profile constrained by geologic data. The model is a one-dimensional line load that considers flexure of broken elastic plate of finite thickness where all of the loads are located at the free boundary. The broken plate model assumes that there is no transmission of stress across the fault separating the hanging wall from the footwall.

Flexure of a broken elastic plate as defined in our model is described in detail by Turcotte and Schubert (1982). The general analytic solution for the flexure of a thin, perfectly elastic plate is

$$w(x) = \left[A \sin\left(\frac{x}{\alpha}\right) + B \cos\left(\frac{x}{\alpha}\right) \right] \exp\left(-\frac{x}{\alpha}\right) \tag{10}$$

The flexural wavelength (α) is

$$\alpha = \left(\frac{4D}{\rho_m g}\right)^{1/4} \tag{11}$$

and the flexural rigidity (D) is

$$D = Eh^3/(12(1 - \nu^2)) \tag{12}$$

where ρ_m is the density of the mantle (the inviscid substrate beneath the elastic plate), E is the plate elasticity (Young's modulus), h is the plate elastic thickness, and ν is Poisson's ratio. The load is a vertical shear force (ν_0) reflecting the combination of sediment infill of the hanging wall and incision of the footwall block

$$\nu_0 = (V_{ifp} + V_{ife})g(\rho_c - \rho_s) + V_e g \rho_c \tag{13}$$

where ρ_c is the density of the crust, ρ_s is the density of the infill, g is the acceleration of gravity, V_{ifp} is the volume of sediments presently infilling the hanging wall, V_{ife} is the volume of sediments previously infilling the hanging wall, but subsequently eroded away, and V_e is the volume of rock eroded from the footwall.

The maximum amplitude of vertical deflection w_0, that occurs at the point of unloading is given by

$$w_0 = \nu_0 \alpha^3/(4D) \tag{14}$$

Similarly, the vertical deflection of the surface of the plate as a function of distance away from the point of unloading ($w(x)$) is

$$w(x) = w_0(\exp(-x/\alpha))\cos(x/\alpha) \tag{15}$$

The model uses the physical parameters in table 2.

TABLE 2

Physical constants of the flexural model

Parameter	Definition	Value
E	plate elasticity	$7 * 10^{10}$ Pa
g	acceleration of gravity	9.81 m s^{-1}
ρ_c	density of the crust	2700 kg m^{-3}
ρ_{sed}	density of the sediments	2100 kg m^{-3}
ρ_m	density of the mantle	3300 kg m^{-3}
ν	Poisson's Ratio	0.25

The Sila Plateau rim is raised between 300 and 400 m above the plateau interior on the residual topography cross-section (fig. 9). Substituting these values into equation (10) and solving it for α where $x = 0$ returns a value of the effective elastic thickness (h) in the range of 3000 to 4000 m. We use these values as a guide to the range of reasonable elastic thicknesses that can be forward modeled with estimates of the volume of sediment infill at the hanging wall and of the eroded rock at the footwall (table 3). The results are compared directly to the residual topography of the plateau (fig. 10). Values of V_{ifp} (volume of sediments presently infilling the hanging wall), V_{ife} (volume of sediments filling the hanging wall, but subsequently eroded away) are calculated directly from known, map-scale geologic constraints. The value for V_e (volume of rock eroded from the footwall) is determined by calculating the 2-D unit volume of rock removed by erosion in the footwall along the east-west cross-section between the actual land surface and the topographic envelope.

Model results for both the north-south cross section and east-west cross section show that the elevation of the Sila Plateau rim can in part be explained by flexural uplift of an unloaded footwall where compensation is in the crust and effective elastic thicknesses lie between 3 and 10 km (fig. 10). This effective elastic thickness is consistent with crustal-scale flexure of plateau margins (Masek and others, 1994a) or rift-flank footwall uplifts (Masek and others, 1994b; Brown and Phillips, 1999; Roy and others, 1999). Perhaps more important than the effect of elastic thickness on plateau margin uplift is the presence or absence of erosional unloading of the footwall. For both the north-south and east-west oriented cross sections, it is footwall erosion that plays the dominant role in driving flexural uplift. Although the fault bounding the Crati valley along Sila's western flank is more active than the fault bounding the northern, Ionian flank, tectonic unloading appears to be subordinate to the effects of

TABLE 3

Vertical deflection w_0 at the point of unloading ($x = 0$ m) obtained solving equation (10) with different values of plate elastic thickness (h)*.

Plate elastic thickness h (m)	Vertical deflection at unloading point w_0 (m)
5000	303.73
4000	359.28
3000	445.55
2000	603.63

*In the calculation the values of V_{ifp} (volume of sediments presently infilling the hanging wall), V_{ife} (volume of sediments filling the hanging wall, but subsequently eroded away), and V_e (volume of rock eroded from the footwall) are respectively $1 * 10^7$, $2 * 10^6$, and $3 * 10^6$.
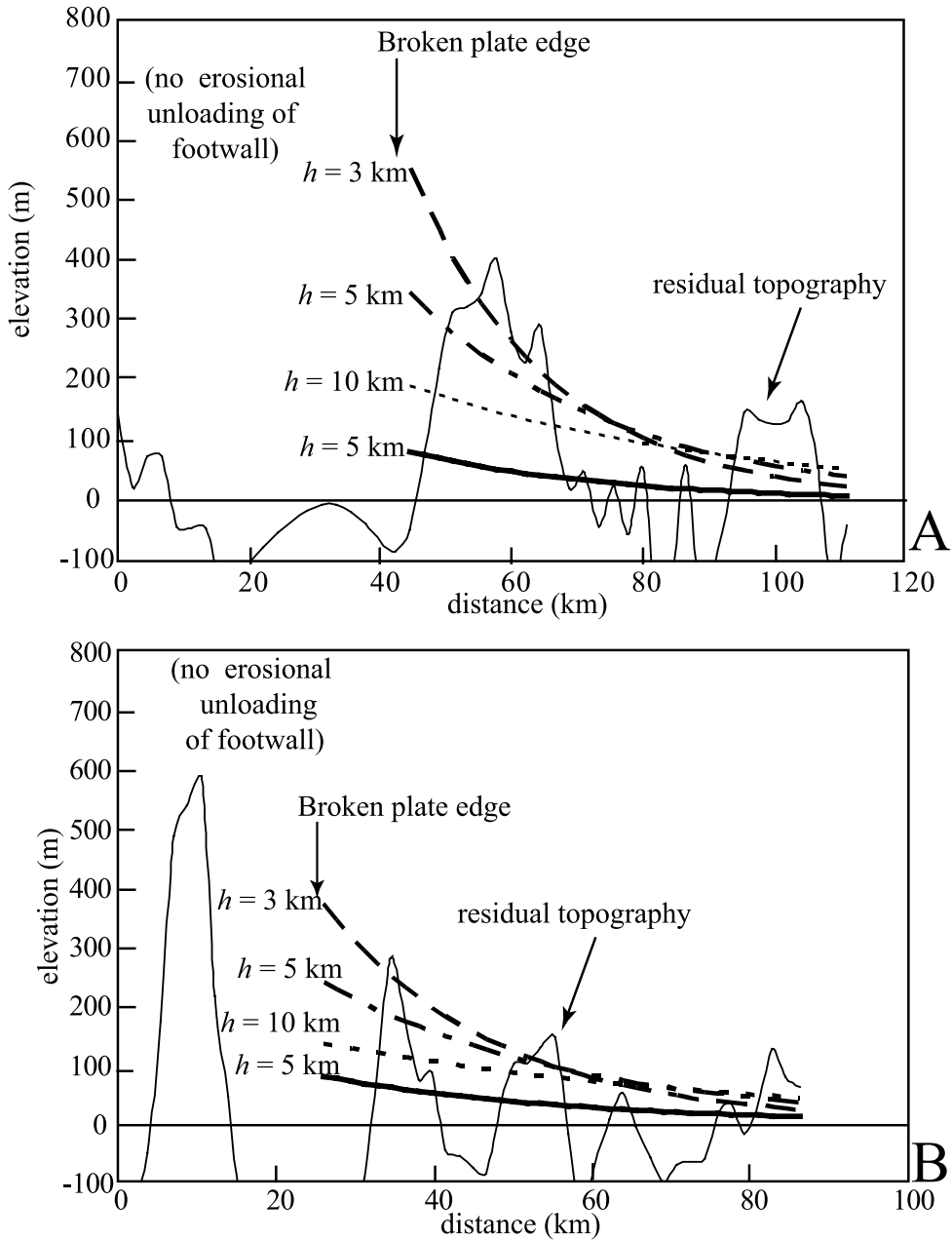
Fig. 10. Results of flexure modeling. (A) Flexural uplift of the north flank of Sila modeled along the north-south cross-section (shown in figure 9). Residual topography is shown by the thin, solid line. Model results using the parameters and loads of tables 2 and 3 are shown for an elastic plate 3 km thick (dotted line), 5 km thick (dash-dotted line) and 10 km thick (dashed line). Model results for a 5 km thick elastic plate and no erosional unloading of the footwall is shown by the thick solid line. (B) Modeling results for the east-west cross section (shown in figure 8B, less the residual relief information). Lines and symbols as in (A) above.

erosional dissection of the plateau rim. There is a greater degree of fluvial dissection along the northern flank ($8.5*10^6$ m^2 of unit cross-section area) with respect to the western flank ($5.3*10^6$ m^2 of unit cross section area). Given the strong dependency between flexural amplitude and erosion, the relative degree of drainage dissection and integration across the plateau margins should have a strong feedback with plateau margin uplift and resulting topography. The amount of actual flexural uplift is thus best reflected in the relief (dissection) of the plateau margin and/or the residual topography rather than the raw topography.

<div align="center">DISCUSSION</div>

Implication of Active Tectonics for Geomorphic and Drainage Evolution of Sila

The results of our topographic analysis of the Sila Massif indicates a geomorphology and landscape dominated by active tectonics acting over a variety of spatial and temporal scales. Landscape evolution is influenced by crustal extension and normal faults, their associated deformation of footwall block tilting, and plateau rim flexural uplift. These local tectonic controls are superimposed on a broader, longer wavelength uplift of the entire Calabrian arc that, because of base level fall, appears to be driving an aggressive drainage integration and dissection of Sila.

The northern portion of the Sila Massif is characterized by a high-standing plateau surrounded by a more elevated edge and external flanks deeply incised by streams (figs. 2, 5, 7, and 8). The general steep, low concavity ratio of the stream long profiles, and the high hypsometry and high elongation ratios are consistent with relatively youthful, actively uplifted watersheds. Modeled long profiles suggest that streams that have successfully breached the plateau rim as well as those that traverse active faults are steeper than those that do not breach the rim and do not cross active faults. The relatively steep, less concave, high *SL* index (table 1, fig. 6A and B) Trionto and Mucone profiles are counterintuitive from the perspective that the lower, modeled parts of these channels might be expected to be less steep given their considerable upstream drainage area. If the integration across the Sila rim is a relatively recent event, then the steep profiles can be explained as simply not having enough time to adjust to their increased discharge, although the deep gorges associated with these rivers are consistent with rapid incision of channels seeking out a new, lower base level of erosion.

Contributing as much if not more to the differences in profile concavity and steepness for streams draining the northern flank of the plateau is the presence of the actively uplifting OD-ridge. The highest mapped *SL* values (fig. 6) correspond well with the highest relief values, (fig. 5) and the locations of knickpoints and knickzones on the long profiles (fig. 4). These knickpoints further coincide with mapped faults, but poorly with known rock-type changes. The OD-ridge is in fact bound on its southwestern flank by an active fault (Molin, ms, 2001; Galli and Bosi, 2003), and its uplift may be inhibiting the Cino and Colognati Rivers, in particular, from breaching the plateau rim. All of the streams are shifted away radially from center of highest relief of the OD-ridge (fig. 6C). The residual high uplift has also influenced the course and incision of the Trionto River, whose long profile shows a knickzone coincident with the ridge followed upstream by a low-gradient reach. These observations also suggest that the Trionto profile continues to adjust to an actively uplifting ridge and probably only recently breached the plateau rim.

The fault that bounds the OD-ridge is just one of many extensional faults that help crudely define the boundary of the Sila Plateau. Collectively, these faults contribute to unload the plateau rim and, together with fluvial dissection, drive flexural uplift of the plateau flanks (fig. 10). A feedback between fluvial dissection and flexural uplift helps pin the location of the drainage divide between the external and internal drainages

(Tucker and Slingerland, 1994). In this way, the low relief interior of Sila can be preserved even when it has been uplifted far above base level. The flexural feedback mechanism is limited by the wavelength of flexural response so eventually, more than just the Mucone and Trionto rivers will likely breach the plateau rim and drain the interior.

On the western flank of the Sila Massif, the influence of the N-S extensional faults that border the Crati River Valley, is well expressed by the drainages. The Mucone River has a very straight long profile downstream of Cecita Lake (fig. 4). This straight segment corresponds to an area of high *SL* indices and of high local relief (figs. 5 and 6). Moreover the highest *SL* index peak just upstream of the plateau edge, whose location is in agreement with a slight convexity in the long profile. We interpret this location as the last remnant of the eroded plateau edge. The Mucone River may have grown to be the master stream draining the western flank of Sila, ultimately integrating its drainage into the interior because its course followed several bedrock fractures. The barbed, right-angle bends in the Mucone headwaters are consistent with recent stream capture of both the Sila internal drainage as well as the former headwaters of the Trionto and Coriglianeto rivers by the Mucone tributary that first breached the plateau rim. The rapid increase in watershed area following the capture of the plateau drainage has driven the aggressive Mucone River incision of the western flank of Sila and concurrent delivery of a large sediment load, much of which forms a huge alluvial fan across the Crati Valley floor at the Mucone-Crati river confluence.

The influence of tectonics on the drainage pattern of the western flank of the Sila is shown also by the asymmetry of drainage basins (fig. 6C). Most of the stream trunk channels are shifted northward, probably as a consequence of either greater or more recent activity on the southern segment of the eastern Crati Valley fault system. The relative activity of these structures and propagation of activity to the south is also supported by the higher values of residual relief just south of Gidora River (figs. 5D and 8) and by low values of local relief right at the foot of this flank caused by low incision across the fault scarps (fig. 8).

Further to the northwest, the plateau edge is partially absent around the head of the Coriglianeto River. This stream has carved a valley into the Sila northern flank, and probably drained at least part of the plateau interior, but its deep headward erosion never incised the plateau floor. When the Mucone breached the rim and captured much of the plateau drainage, the Coriglianeto headwaters were beheaded. The subsequent loss of drainage area is suggested by thick (60 m) fan deposits presently 100 to 300 m above base level (Molin, ms, 2001). These represent a time before the beheading when the Coriglianeto was transporting more sediment than at present.

Conceptual Model of Landscape Evolution of the Sila Massif

The topographic analysis of the northern portion of the Sila Massif has highlighted the strong influence of active tectonics on the landscape evolution of this area. We cast these results into the larger context of Apennine uplift and landscape evolution to suggest a model for the geologic and landscape evolution of this part of Calabria from the Miocene to the Present. The reconstruction is supported by published data about unroofing, geology and stratigraphy, and absolute uplift of rocks with respect to sea level.

During the lower and middle Miocene, the Sila Massif was exhumed by both syn- and late-orogenic extensional tectonics and erosional denudation (Thomson, 1994; Rossetti and others, 2001). La Sila must have been relatively high-standing at this time because, as basins opened in the newly-formed backarc, several allostatigraphic packages of continental and marine sediments were deposited by streams with a Sila provenance (Ogniben, 1973; Amodio-Morelli and others, 1976; Ortolani and others, 1979; Romeo and Tortorici, 1980; Sorriso-Valvo and Sylvester, 1993; Colella, 1995;

Argentieri and others, 1998; Critelli and Le Pera, 1998). A remnant of this erosional exhumation, if still preserved in the landscape, would be the Sila upland. The deep weathering of the plateau surface, with saprolite tens of meters thick, support the antiquity of this surface which was likely very subdued in relief by the end of the Miocene or beginning of the Pliocene.

Crustal extension increased markedly in the early Pliocene, affecting mostly the interior portion of the forearc by increasing the subsidence of the existing basins and inducing the opening of Crati basin (Lanzafame and Tortorici, 1981; Colella and others, 1987; Moretti, 1993). Here the footwall uplift of the active N-S faults that form the eastern border of the basin initiated the flexural uplift of what would ultimately evolve to become the Sila plateau rim. Similarly, on the Ionian flank of the massif, the activity of NW-SE faults produced the north-eastern edge of the plateau. In the subsiding basins that were located in the hanging walls of these faults, marine siliciclastics with a Sila provenance were deposited (Vezzani, 1968; Ogniben, 1973; Colella and others, 1987; Critelli, 1990; Moretti, 1993). Adjacent to faults bordering Sila, these sediments commonly interfinger with coarse fluvial facies, consistent with the incision of a steep topographic escarpment. The lack of any marine deposits on the plateau indicates that there was enough local uplift or topography of Sila at this time to keep the present plateau surface above sea level.

Extensional basins flanking the plateau continued to subside until the end of lower Pleistocene, when the study area was affected by a regional uplift that raised both the Sila Massif and the surrounding basins above sea level (Vezzani, 1968; Lanzafame and Tortorici, 1981; Ciaranfi and others, 1983; Moretti, 1983; Boccaletti and others, 1984; Colella and others, 1987; Tortorici and others, 1995; Moretti and Guerra, 1997). The basins rapidly filled with fluvial deposits derived from the invigorated fluvial dissection of the plateau flanks. This regional uplift of rocks and the land surface is similar to that argued for the entire Apennines (Ciaranfi and others, 1983; Colella and others, 1987; Dramis, 1992; Moretti, 1993; Tortorici and others, 1995; Moretti and Guerra, 1997; Calamita and others, 1999; Coltorti and Pieruccini, 2000; Feroni and others, 2001), has an uncertain origin perhaps related to a geodynamic change in the rate, angle, or tear of the subducting slab (Moretti, 1993; Giunchi and others, 1996; Moretti and Guerra, 1997; Buiter and others, 1998; Carminati and others, 1998; Calamita and others, 1999; Gvirtzman and Nur, 1999, 2001; Wortel and Spakman, 2000). Ultimately, this middle-late Pleistocene uplift produced the progressive emergence of the surrounding basins and successive erosion of marine sediments. At the same time the significant fall in base level around Sila fostered stream incision, elongation of the headwaters beyond the flexurally-uplifted plateau rim, and integration of the drainage atop the plateau's upland surface. These processes were influenced by local tectonics such as rapid recent uplift of the OD-ridge that favored first the formation of the paleo-Cecita Lake and then the Mucone River capture of upland surface drainage at the expense of the Trionto or adjacent drainages.

In the middle-upper Pleistocene, the interaction between regional uplift, glacio-eustasy, and climatically-modulated changes in sediment yield formed alluvial and marine terraces in the Crati Valley and along the Ionian coast. These terraces record an uplift rate of 0.6 to 1.0 mm/yr in the last 100 kyr (Lanzafame and Tortorici, 1981; Colella and others, 1987; Gliozzi, ms, 1988; Carobene and others, 1989; Carobene and Dai Prà, 1990; Palmentola and others, 1990; Moretti, 1993; Cucci and Cinti, 1998; Mauz and Hassler, 2000; Molin and others, 2002). Our regional analysis of relief expressed in the swath cross profiles (fig. 8) and in the residual topography maps (fig. 5D) indicates that the regional Quaternary uplift has a complicated interaction with the rates of local active faulting. In places like the subsiding Crati valley, fluvial dissection appears to be responding primarily to regional uplift as Quaternary fluvial sediments are now being

incised. In contrast, in places like the OD-ridge and the Catena Costiera, rapid footwall uplift completely dominates the courses and gradients of the drainages. Uplift of the Catena Costiera may be very recent and rapid in comparison to the flanks of the Sila Massif given the strong contrast in local relief imposed by juvenile versus mature drainages respectively (fig. 8).

<div align="center">CONCLUSIONS</div>

Topography reflects the interaction between tectonics that induces rock mass movements, and geomorphic processes that rearrange materials on the resulting relief (Beaumont and others, 2000; Hovius, 2000). In active tectonic regions landscapes are a first-order approximation of tectonic processes acting at various length scales (Mayer, 2000). Our topographic analyses on a portion of the southern Apennines, the Sila Massif in Calabria, reveals those geomorphic features most sensitive to rapid uplift in the context of an actively deforming forearc and helps constrain a general model for how and when topography emerged. We summarize our results as follows:

1) The landscape of central Calabria is shaped by extensional tectonics superimposed on a broader, more regional uplift of the entire forearc. Actively incising streams, a poorly integrated interior drainage, a deeply weathered, low-relief plateau upland, a coarsening-up and progressively more fluviatile basin stratigraphy, and lack of any marine deposits younger than middle Pleistocene all suggest rapid emergence of Calabria since the middle Pleistocene.

2) Stream long profiles and concavities measured by two separate methods coupled with Hack stream gradient indices were among the most useful morphometric indices for elucidating tectonic deformation and uplift at length scales consistent with active faults. Swath cross-profiles and relief residual maps were among the most useful metrics for capturing tectonic deformation operating at flexural and regional uplift length scales.

3) The core of central Calabria is the Sila Massif. The high-standing plateau located on the top of the massif remains relatively undeformed with respect to its margins, delimited by extensional faults. Extensional collapse around Sila has unloaded the plateau rim, resulting in footwall flexural uplift. This flexural uplift is most sensitive to stream incision and erosional unloading of the footwall that leads to a feedback between uplift and the ability of an individual stream to breach the plateau rim and drain its interior. The drainage divide is locally pinned between steep rivers draining the plateau flanks and a low-relief drainage system in the plateau interior.

4) On the northern flank of Sila, the formation of the plateau rim has been magnified by the activity of extensional faults that, located just east of Cecita Lake, drop the plateau floor. The activity of both fault systems induced the local uplift of a NW-SE trending horst (the OD-ridge) that has influenced drainage network evolution.

5) Locally, streams exploiting faults and fault zones have been successful in breaching the plateau rim and pirate the headwaters of adjacent streams, allowing the onset of plateau interior dissection.

6) The previous observations underscore the significant lag times a landscape may endure in transforming from one tectonic and base level condition to another. For the Calabrian forearc, the Sila interior represents a portion of the landscape slow to adjust to the modern tectonic and base level setting. This is why a landscape in a tectonically active region may still retain vestiges of the formerly dominant base level (low-relief landscape) and processes (deeply chemically weathered soils) out of equilibrium with modern base level and weathering processes.

The general reconstructed geomorphic evolution of the Calabrian forearc shares many characteristics in common with the geomorphic evolution of other parts of the Apennines. We conclude that the conditions driving regional uplift of Calabria in the Quaternary are not restricted to this part of the chain but rather are part of the highly debated geodynamic mechanisms responsible for the generation of during the long orogenic history of this range.

REFERENCES

Amato, A., and Cinque, A., 1999, Erosional surfaces of the Campano-Lucano Apennines (S. Italy): genesis, evolution, and tectonic implications: Tectonophysics, v. 315, p. 251–267.

Amodio-Morelli, L., Bonardi, G., Colonna, V., Dietrich, D., Giunta, G., Ippolito, F., Liguori, V., Lorenzoni, S., Paglianico, A., Perrone, V., Piccarreta, G., Russo, M., Scandone, P., Zanettin Lorenzoni, E., and Zuppetta, A., 1976, L'arco calabro-peloritano nell'orogene appennino-maghrebide: Memorie della Società Geologica Italiana, v. 17, p. 1–60.

Argentieri, A., Mattei, M., Rossetti, F., Argnani, A., Salvini, F., and Funiciello, R., 1998, Tectonic evolution of the Amantea basin (Calabria, southern Italy): comparison in-land and off-shore data: Annales Tectonicae, v. 12 (1-2), p. 79–96.

Argnani, A., Bernini, M., Di Dio, G. M., Papani, G., and Rogledi, S., 1997, Stratigraphic record of the crustal-scale tectonics in the Quaternary of the northern Apennines (Italy): Il Quaternario, v. 10, p. 597–604.

Ascione, A., and Cinque, A., 1999, Tectonics and erosion in the long term relief history of the southern Apennines (Italy): Zeitschrift für Geomorphologie N. F., Supplementbände 118, p. 1–16.

Beaumont, C., Kooi, H., and Wilett, S., 2000, Coupled tectonic-surface process models with applications to rift margins and collisional orogens, *in* Summerfield, M. A., editor, Geomorphology and Global Tectonics: New York, John Wiley and Sons, p. 29–55.

Bertotti, G., Cloetingh, S., Spadini, G., Podladchickov, Y., and Picotti, V., 1997, Kinematics and dynamics of the fast continental rifting and passive margin formation in the Tyrrhenian Sea (Mediterranean): Abstract with programs – Geological Society of America, v. 29 (6), p. 317.

Boccaletti, M., Nicolich, R., and Tortorici, L., 1984, The Calabrian arc and the Ionian sea in the dynamic evolution of the central Mediterranean: Marine Geology, v. 55, p. 219–245.

Bousquet, J. C., 1973, La Tectonique 0recente de l'Apennin calabro-lucanien dans son cadre geologique et geophysique: Geologica Romana, v. 12, p. 1–104.

Brancaccio, L., Pescatore, T., Sgrosso, I., and Scarpa, R., 1984, Geologia regionale, in Pescatore T., editor, Lineamenti di geologia regionale e tecnica - Le aree colpite dal terremoto del 23 Novembre 1980, FORMEZ.

Brown, C. D., and Phillips, R. J., 1999, Flexural rift flank uplift at the Rio Grande rift, New Mexico: Tectonics, v. 18, p. 1275–1291.

Buiter, S. J. H., Wortel, M. J. R., and Govers, R., 1998, The role of subduction of the Apennines foreland basin: Tectonophysics, v. 296, p. 249–268.

Calamita, F., Coltorti, M., Pieruccini, P., and Pizzi, A., 1999, Evoluzione strutturale e morfogenesi plio-quaternaria dell'Appennino umbro-marchigiano tra il preappennino umbro e la costa adriatica: Bollettino della Società Geologica Italiana, v. 118, p. 125–139.

Carminati, E., Wortel, M. J. R., Spakman, W., and Sabadini, R., 1998, The role of slab detachment processes in the opening of the western-central Mediterranean basin: some geological and geophysical evidence: Earth and Planetary Science Letters, v. 160, p. 651–665.

Carminati, E., Giunchi, C., Argnani, A., Sabadini, R., and Fernandez, M., 1999, Plio-Quaternary vertical motion of the northern Apennines: Insights from dynamic modeling: Tectonics, v. 18, p. 703–718.

Carobene, L., and Dai Prà, G., 1990, Genesis, chronology and tectonics of the Quaternary marine terraces of the Tyrrhenian coast of the northern Calabria (Italy): their correlation with climatic conditions: Il Quaternario, v. 3 (2), p. 75–94.

Carobene, L., Mengani, M. E., and Oliviero, M., 1989, Superfici terrazzate pleistoceniche nella media valle del Fiume Crati (Calabria): Il Quaternario, v. 2 (1), p. 15–39.

Castellarin, A., Eva, C., Gigli, C., and Vai, G. B., 1985, Analisi strutturale del Fronte Appenninico Padano: Giornale di Geologia, v. 47, p. 47–76.

Cavinato, G. P., and De Celles, P. G., 1999, Extensional basins in the tectonically bimodal central Apennines fold-thrust belt, Italy: Response to corner flow above a subducting slab in retrograde motion: Geology, v. 27 (10), p. 955–958.

Ciaranfi, N., Ghisetti, F., Guida, M., Iaccarino, G., Pieri, P., Rapisardi, L., Ricchetti, G., Torre, M., Tortorici, L., and Vezzani, L., 1983, Carta neotettonica dell'Italia meridionale, C.N.R. P.F.G., v. 515, Bari, p. 62.

Colella, A., 1995, Sedimentation, deformational events and eustacy in the perityrrhenian Amantea Basin: preliminary synthesis: Giornale di Geologia, v. 57 (1-2), p. 179–193, 8ff.

Colella, A., De Boer, L., and Nio, S. D., 1987, Sedimentology of a marine intermontane Pleistocene Gilbert-type fan-delta complex on the Crati Basin, Calabria, southern Italy: Sedimentology, v. 34, p. 721–736.

Coltorti, M., and Pieruccini, P., 2000, A late lower Pliocene planation surface across the Italian Peninsula: a key tool in neotectonic studies: Journal of Geodynamics, v. 29, p. 323–328.

Cristofolini, R., Ghisetti, F., Scarpa, R., and Vezzani, L., 1985, Character of the stress field in the Calabrian arc and southern Apennines (Italy) as deduced by geological, seismological and volcanological information: Tectonophysics, v. 117, p. 39–58.

Critelli, S., 1990, Geological setting of the Trionto River basin, *in* Symposium on geomorphology of active tectonic area - Excursion guidebook, IGU-COMTAG and CNR, Cosenza, June 1990, p. 67–70.

Critelli, S., and Le Pera, E., 1998, Post-Oligocene sediment-dispersal systems and unroofing history of the Calabrian microplate, Italy: International Geology Review, v. 40 (7), p. 609–637.

Cucci, L., and Cinti, F. R., 1998, Regional uplift and local tectonic deformation recorded by the Quaternary marine terraces on the Ionian coast of northern Calabria: Tectonophysics, v. 292, p. 67–83.

Demoulin, A., 1998, Testing the tectonic significance of some parameters of longitudinal river profiles: the case of the Ardenne (Belgium, NW Europe): Geomorphology, v. 24, p. 189–208.

Dietrich, D., 1976, La geologia della Catena Costiera calabra tra Cetraro e Guardia Piemontese: Memorie della Società Geologica Italiana, v. 17, p. 61–121.

Dramis, F., 1992, Il ruolo dei sollevamenti tettonici a largo raggio nella genesi del rilievo appenninico: Studi Geologici Camerti, volume speciale (1992/1), p. 9–15.

Dramis, F., Gentili, B., and Pambianchi, G., 1990, Geomorphological scheme of the River Trionto basin, *in* Symposium on geomorphology of active tectonic area - Excursion guidebook, IGU-COMTAG and CNR, Cosenza, June 1990, p. 63–66.

Faccenna, C., Mattei, M., Funiciello, R., and Jolivet, L., 1997, Styles of back-arc extension in the Central Mediterranean: Terra Nova, v. 9, p. 126–130.

Faccenna, C., Funiciello, F., Giardino, D., and Lucente, P., 2001, Episodic back-arc extension during restricted mantle convection in the Central Mediterranean: Earth and Planetary Science Letters, 187 (1-2), p. 105–116.

Feroni, A. C., Leoni, L., Martelli, L., Martinelli, P., Ottria, G., and Sarti, G., 2001, The Romagna Apennines, Italy; an eroded duplex: Geological Journal, v. 36, p. 39–54.

Flint, J. J., 1974, Stream gradient as a function of order, magnitude, and discharge: Water Resources Research, v. 10, p. 969–973.

Galli, P., and Bosi, V., 2003, Catastrophic 1638 earthquakes in Calabria (southern Italy): New insights from paleoseismological investigation: Journal of Geophysical Research, v. 108 (B1), 2004, doi: 10.1029/2001JB001713.

Gardner, T. W., Back, W., Bullard, T. F., Hare, P. W., Kesel, R. H., Lowe, D. R., Menges, C. M., Mora, S. C., Pazzaglia, F. J., Sasowsky, I. D., Troester, J. W., and Wells, S. G., 1987, Central America and the Caribbean, *in* Graf, W. L., editor, Geomorphic systems of North America: Boulder, Colorado, Geological Society of America, Centennial Special Volume 2, p. 343–401.

Ghisetti, F., 1979, Evoluzione neotettonica dei principali sistemi di faglie della Calabria centrale: Bollettino della Società Geologica Italiana, v. 98, p. 387–430.

Ghisetti, F., and Vezzani, L., 1982, Different styles of deformation in the Calabrian arc (southern Italy): implications for a seismotectonic zoning: Tectonophysics, v. 85, p. 149–165.

Giunchi, C., Sabadini, R., Boschi, E., and Gasperini, P., 1996, Dynamic models of subduction: geophysical and geological evidence in the Tyrrhenian Sea: Geophysical Journal International, v. 126, p. 555–578.

Gliozzi, E., ms, 1988, I terrazzi marini del Pleistocene superiore della penisola di Crotone: Ph.D. thesis, Università degli Studi di Napoli, Naples, Italy, 153 p.

Gueguen, E., Doglioni, C., and Fernandez, M., 1998, On the post-25 Ma geodynamic evolution of the western Mediterranean: Tectonophysics, v. 298 (1-3), p. 259–269.

Gvirtzman, Z., and Nur, A., 1999, Plate detachment, asthenosphere upwelling, and topography across subduction zones: Geology, v. 27 (6), p. 563–566.

——— 2001, Residual topography, lithospheric structure and sunken slab in the central Mediterranean: Earth and Planetary Science Letters, v. 187, p. 117–130.

Hack, J. T., 1957, Studies of longitudinal profiles in Virginia and Maryland: U. S. Geological Survey Professional Paper 294-B, p. 45–97.

——— 1973, Stream analysis and stream-gradient index: U. S. Geological Survey Journal of Research, v. 1 (4), p. 421–429.

Henderson, G., 1970, Carta Geologica della Calabria: CASMEZ sheet 230, scale 1:25000.

Hippolyte, J. C., Angelier, J., and Roure, F., 1994, A major geodynamic change revealed by Quaternary stress patterns in the Southern Apennines (Italy): Tectonophysics, v. 230 (3-4), p. 199–210.

Hovius, N., 2000, Macroscale process systems of mountain belt erosion, *in* Summerfield, M. A., Geomorphology and Global Tectonics: New York, John Wiley and Sons, p. 77–105.

Howard, A. D., and Kerby, G., 1983, Channel changes in badlands: Geological Society of America Bulletin, v. 94, p. 739–752.

Hurtrez J. E., and Lucareau F., 1999, Lithological control on relief and hypsometry in the Hérault drainage basin (France): Earth and Planetary Sciences, v. 328, p. 687–694.

Jolivet, L., and Faccenna, C., 2000, Mediterranean extension and the Africa-Eurasia collision: Tectonics, v. 19 (6), p. 1095–1106.

Keller, E. A., and Pinter, N., 1996, Active Tectonics: Upper Saddle River, New Jersey, Prentice Hall, p. 338.

Kirby, E. and Whipple, K. X., 2001, Quantifying differential rock-uplift rates via stream profile analysis: Geology, v. 29, p. 415–418.

Knott, S. D., 1987, The Liguride Complex of southern Italy – a Cretaceous to Paleogene accretionary wedge: Tectonophysics, v. 142, p. 217–226.

Knott, S. D., and Turco, E., 1991, Late Cenozoic kinematics of the Calabrian arc, southern Italy: Tectonics, v. 10 (6), p. 1164–1172.

Lanzafame, G., and Tortorici, L., 1981, La tettonica recente della Valle del Fiume Crati (Calabria): Geografia Fisica e Dinamica Quaternaria, v. 4, p. 11–21.

Lanzafame, G., Spadea, P., and Tortorici, L., 1979, Mesozoic ophiolites of the northern Calabria and Lucanian Apennine (southern Italy): Ofioliti, v. 4 (2), p. 173–182.

Lavecchia, G., Brozzetti, F., Barchi, M., Menichetti, M., and Keller, J. V. A., 1994, Seismotectonic zoning in east-central Italy deduced from an analysis of the Neogene to present deformations and related stress fields: Geological Society of America Bulletin, v. 106, p. 1107–1120.

Leopold, L. B., Wolman, M. G., and Miller, J. P., 1964, Fluvial Processes in Geomorphology: San Francisco and London, W. H. Freeman and Company, p. 522.

Le Pera, E., and Sorriso-Valvo, M., 2000, Weathering and morphogenesis in a Mediterranean climate, Calabria, Italy: Geomorphology, v. 34, p. 251–270.

Lonergan, L., and White, N., 1997, Origin of the Betic-Rif mountain belt: Tectonics, v. 16, p. 504–522.

Mackin, J. H., 1948, Concept of the graded river: Geological Society of America Bulletin, v. 59, p. 463–512.

Malinverno, A., and Ryan, W. B. F., 1986, Extension in the Tyrrhenian Sea and shortening in the Apennines as results of arc migration driven by sinking of the lithosphere: Tectonics, v. 5, p. 227–245.

Mantovani, E., Albarello, D., Tamburelli, C., and Babbucci, D., 1996, Evolution of the Tyrrhenian basin and surrounding regions as a result of the Africa-Eurasia convergence: Journal of Geodynamics, v. 21 (1), p. 35–72.

Masek, J. G., Isakcs, B. L., Gubbels, T. L., and Fielding, E. J., 1994a, Erosion and tectonics at the margins of continental plateaus: Journal of Geophysical Research, v. 99 (B7), p. 13941–13956.

Masek, J. G., Isakcs, B. L., and Fielding, E. J., 1994b, Rift flank uplift in Tibet: evidence for viscous lower crust: Tectonics, v. 13 (2), p. 659–667.

Mauz, B., and Hassler, U., 2000, Luminescence chronology of Late Pleistocene raised beaches in southern Italy: new data of relative sea-level changes: Marine Geology, v. 170, p. 187–203.

Mayer, L., 2000, Application of digital elevation models to macroscale tectonic geomorphology, *in* Summerfield, M. A., Geomorphology and Global Tectonics: New York, John Wiley and Sons, p. 15–27.

Molin, P., ms, 2001, L'analisi topografica come strumento per definire il ruolo morfogenetico della tettonica distensiva e del sollevamento regionale in un transetto della Calabria settentrionale: Ph.D. thesis, Università degli Studi "Roma Tre", Rome, Italy, 140 p.

Molin, P., Dramis, F., and Lupia Palmieri, E., 2002, The Plio-Quaternary uplift of the Ionian northern Calabria coastal belt between Corigliano Calabro e Capo Trionto: Studi Geologici Camerti, v. 2002, p. 135–145.

Monaco, C., and Tortorici, L., 2000, Active faulting in the Calabrian arc and eastern Sicily: Journal of Geodynamics, v. 29, p. 407–424.

Moretti, A., 1993, Note sull'evoluzione tettono-stratigrafica del bacino crotonese dopo la fine del Miocene: Bollettino della Società Geologica Italiana, v. 112, p. 845–867.

Moretti, A., and Guerra, I., 1997, Tettonica dal Messiniano ad oggi in Calabria: implicazioni sulla geodinamica del sistema Tirreno-Arco calabro: Bollettino della Società Geologica Italiana, v. 116, p. 125–142.

Mostardini, F., and Merlini, S., 1988, Appennino centro-meridionale. Sezioni geologiche e proposta di modello strutturale: Memorie della Società Geologica Italiana, v. 35, p. 177–202.

Moussat, E., Angelier, J., Mascle, G., and Rehault, J. P., 1986, L'ouverture de la Mer Tyrrhénienne et la tectonique de faille néogènè quaternaire en Calabre: Giornale di Geologia, v. 48/1-2, p. 63–75.

Negredo, A. M., Barba, S., Carminati, E., Saladini, R., and Giunchi, C., 1999, Contribution of numeric dynamic modeling to the understanding of the seismotectonic regime of the northern Apennines: Tectonophysics, v. 315, p. 15–30.

Ogniben, L., 1973, Schema geologico della Calabria in base ai dati odierni: Geologica Romana, v. 12, p. 243–585.

Ortolani, F., Torre, M., and Di Nocera, S., 1979, I depositi altomiocenici del bacino di Amantea (Catena Costiera calabra): Bollettino della Società Geologica Italiana, v. 98, p. 559–587.

Palmentola, G., Carobene, L., Mastronuzzi, G., and Sansò, P., 1990, I terrazzi pleistocenici della Penisola di Crotone (Calabria): Geografia Fisica e Dinamica Quaternaria, v. 13, p. 75–80.

Patacca, E., and Scandone, P., 1989, Post-Tortonian mountain building in the Apennines. The role of the passive sinking of a relic lithospheric slab, *in* Boriani, A., Bonafede, M., Piccardo, G. B., and Vai, G. B., editors, The lithosphere in Italy: Accademia Nazionale dei Lincei, Roma, p. 157–176.

Patacca, E., Sartori, R., and Scandone, P., 1990, Tyrrhenian basin and Apenninic arcs: Kinematic relations since late Tortonian times: Memorie della Società Geologica Italiana, v. 45, p. 425–451.

Pazzaglia, F. J., Gardner, T. W., and Merritts, D., 1998, Bedrock fluvial incision and longitudinal profile development over geologic time scales determined by fluvial terraces, *in* Wohl, E., and Tinkler, K., editors, Bedrock Channels: American Geophysical Union, Geophysical Monograph Series, v. 107, p. 207–235.

Romeo, M., and Tortorici, L., 1980, Stratigrafia dei depositi miocenici della Catena Costiera calabra meridionale e della media valle del Fiume Crati (Calabria): Bollettino della Società Geologica Italiana, v. 99, p. 303–318.

Rossetti, F., Faccenna, C., Goffé, B., Monié, P., Argentieri, A., Funiciello, R., and Mattei, M., 2001, Alpine structural and metamorphic signature of the Sila Piccola Massif nappe stack (Calabria, Italy): insights for the tectonic evolution of the Calabria Arc: Tectonics, v. 20 (1), p. 112–133.

Roy, M., Karlstrom, K., Kelley, S., Pazzaglia, F. J., and Cather, S., 1999, Topographic setting of the Rio Grande and Rift, New Mexico: assessing the role of flexural "rift-flank uplift" *in* The Sandia Mountains, New Mexico Geological Society Guidebook, 50th Field Conference, Albuquerque Geology, p. 167–174.

Royden, L., Patacca, E., and Scandone, P., 1987, Segmentation and configuration of the subducted lithosphere in Italy: An important control on the thrust belt and foredeep basin evolution: Geology, v. 15, p. 714–717.

Sartori, R., 1989, Drillings of ODP Leg 107 in the Tyrrhenian Sea: tentative basin evolution compared to deformations in the surrounding chains, *in* Boriani, A., Bonafede, M., Piccardo, G. B., and Vai, G. B., editors, The lithosphere in Italy: Accademia Nazionale dei Lincei, Roma, p. 139–156.

Schumm, S. A., 1956, Evolution of drainage systems and slopes badlands at Perth Amboy, N. J.: Geological Society of America Bulletin, v. 67, p. 597–646.

Schumm, S. A., Mosley, M. P., and Weaver, W. E., 1987, Experimental Fluvial Geomorphology: New York, Wiley Interscience, p. 413.

Schumm, S. A., Dumont, J. F., and Holbrook, J. M., 2000, Active tectonics and alluvial rivers: Cambridge, United Kingdom, Cambridge University Press, p. 276.

Snyder, N. P., Whipple, K. X., Tucker, G. E., and Merritts, D. J., 2000, Landscape response to tectonic forcing: Digital elevation model analysis of stream profiles in the Mendocino triple junction region, northern California: Geological Society of America Bulletin, v. 112, p. 1250–1263.

Sorriso-Valvo, M., 1993, The geomorphology of Calabria - A sketch: Geografia Fisica e Dinamica Quaternaria, v. 16, p. 75–80.

Sorriso-Valvo, M., and Sylvester, A. G., 1993, The relationship between geology and landforms along a coastal mountain front, northern Calabria, Italy: Earth Surface Processes And Landforms, v. 18, p. 257–273.

Strahler, A. N. 1952, Hypsometric (area-altitude) analysis of erosional topography: Geological Society of America Bulletin, v. 63, p. 1117–1141.

–––––– 1957, Quantitative analysis of watershed geomorphology: Transactions American Geophysical Union, v. 38, p. 913–920.

Tarboton, D. G., Bras, R. L., Rodriguez-Iturbe, I., 1989, Scaling and elevation in river networks: Water Resources Research, v. 25, p. 2037–2051.

Thomson, S. N., 1994, Fission track analysis of the crystalline basement rocks of the Oligo-Miocene late-orogenic extension and erosion: Tectonophysics, v. 238, p. 331–352.

Tortorici, L., Monaco, C., Tansi, C., and Cocina, O., 1995, Recent and active tectonics in the Calabrian arc (southern Italy): Tectonophysics, v. 243, p. 37–55.

Tucker, G., and Slingerland, R. L., 1994, Erosional dynamics, flexural isostasy, and long-lived escarpments: A numerical modeling study: Journal of Geophysical Research, v. 99, B6, p. 12,229–12,243.

Turcotte, D. L., and Schubert, G., 1982, Geodynamics, Applications of continuum physics to geological problems: New York, John Wiley and Sons, p. 450.

van Dijk, J. P., and Scheeprs, P. J. J., 1995, Neotectonic rotations in the Calabrian Arc; implications for a Pliocene-Recent geodynamic scenario for the central Mediterranean: Earth Science Review, v. 39 (3-4), p. 207–246.

Vening-Meinesz, F. A., 1950, Les 'grabens' africains, resultat de compression ou de tension dans la croute terrestre?: Bulletin of the Royal Colonian Institute of Belgium, v. 21, p. 539–552.

Vezzani, L., 1968, I terreni plio-pleistocenici del basso Crati (Cosenza): Atti dell'Accademia Gioenia di Scienze Naturali Catania, ser. VI, v. 20, p. 28–84.

Wells, S. G., Bullard, T. F., Menges, C. M., Drake, P. G., Karas, P. A., Kelson, K. I., Ritter, J. B., and Wesling, J. R., 1988, Regional variations in tectonic geomorphology along a segmented convergent plate boundary, Pacific coast of Costa Rica: Geomorphology, v. 1, p. 239–266.

Wernicke, B., and Axen, G., 1988, On the role of isostasy in the evolution of normal fault systems: Geology, v. 16, p. 848–851.

Wezel, F. C., 1986, The pacific island arcs: produced by post-orogenic vertical tectonics?, *in* Wezel, F. C., The Origin of Arcs: New York, Elsevier Sciences Publishers, p. 529–567.

Whipple, K. X., and Tucker, G. E., 1999, Dynamics of the stream power river incision model: Implications for height limits of mountain ranges, landscape response times scales, and research needs: Journal of Geophysical Research, v. 104, p. 17,661–17,674.

Willett, S. D., Slingerland, R., and Hovius, N., 2001, Uplift, shortening, and steady state topography in active mountain belts: American Journal of Science, v. 301, p. 455–485.

Willgoose, G., and Hancock, G., 1998, Revisiting the Hypsometric curve as an indicator of form and process in transport-limited catchment: Earth Surface Processes and Landforms, v. 23, p. 611–623.

Wortel, M. J. R., and Spakman, W., 2000, Subduction and slab detachment in the Mediterranean-Carpathian region: Science, v. 290, p. 1910–1917.